USGS NEHRP Final Technical Report

Award #s G18A00040 and G18A00041

"Earthquake Recurrence on the Banning Strand of the San Andreas Fault: Collaborative Research with California State University San Bernardino and University of California Los Angeles"

Sally McGill

Department of Geological Sciences

California State University, San Bernardino

5500 University Parkway, San Bernardino, CA 92407

Phone: 909-537-3304

Fax: none

Email: smcgill@csusb.edu

Seulgi Moon

Department of Earth, Planetary, and Space Sciences

University of California, Los Angeles

595 Charles E Young Dr E, Los Angeles, CA 90095

Fax: none

Email: sgmoon@ucla.edu

Collaborators: Bryan Castillo, Kate Scharer, Doug Yule, Devin McPhillips, James McNeil, Sourav Saha, Nathan Brown

Award term: 6/21/2018 to 6/20/2020

Research supported by the U.S. Geological Survey (USGS), Department of the Interior, under USGS award number (S. McGill, G18A00040; S. Moon, G18A00041). The views and conclusions contained in this document are those of the authors and should not be interpreted as necessarily representing the official policies, either expressed or implied, of the U.S. Government.

ABSTRACT

We studied a paleoseismic trench excavated in 2017 across the Banning strand of the San Andreas Fault and herein provide the first detailed record of ground-breaking earthquakes on this important fault in Southern California. The trench exposed a ~40-m-wide fault zone cutting through alluvial sand, gravel, silt, and clay deposits. We evaluate the paleoseismic record using a new metric that combines event indicator quality and stratigraphic uncertainty. The most recent paleoearthquake occurred between 730 and 950 cal BP, potentially contemporaneous with the last rupture of the San Gorgonio Pass Fault zone. We interpret five surface rupturing earthquakes since 3.3-2.5 ka and eight earthquakes since 7.1-5.7 ka. It is possible that additional events have occurred but were not recognized, especially in the deeper (older) section of the stratigraphy, which was not fully exposed across the fault zone. We calculate an average recurrence interval of 380–640 years based on four complete earthquake cycles between earthquakes 1 and 5. The average recurrence interval is thus slightly less than the elapsed time since the most recent event at the site and is intermediate between longer intervals published for the San Gorgonio Pass Fault zone (~1600 years) and shorter intervals on both the Mission Creek strand of the San Andreas Fault (~215 years) and Coachella section (~125 years) of the San Andreas Fault.

REPORT

Introduction

The San Andreas Fault (SAF) is the longest (~1300 km) and has the highest slip rate of all faults in California. The northern section of the fault ruptured in 1906, and the south-central section in 1857. Only the southernmost section of the SAF (SSAF) has not ruptured during the historical record. The Banning strand of the SAF is located within a complex portion of the SSAF zone (Figure 1). Within the San Gorgonio Pass region, the fault bends to a west-northwest orientation resulting in a complex zone of transpressional faults (Yule and Sieh, 2003). In addition, faults diverge northward from the SSAF toward the Eastern California Shear Zone (ECSZ) (Figure 1). This geometry triggers many questions about the SSAF system such as (1) How is plate boundary slip accommodated within this region? (2) How have earthquake ruptures in this region made use of the various fault strands within this complex region?

To better characterize the seismic behavior of the SSAF, the temporal behavior of the six faults that make up the SSAF fault zone - the Mission Creek, Mill Creek, Banning, Garnet Hill and San Bernardino strands, and the SGPFZ - must be examined, including the rate of ground-rupturing prehistoric earthquakes. This paper contributes the first detailed record of dates of prehistoric earthquakes on the Banning strand.

We report here: 1) the evidence and ages for eight recent paleoearthquakes on the Banning strand; 2) the average recurrence interval between earthquakes on this strand; and 3) a comparison of the timing of paleoearthquakes on the Banning strand with those on the SGPFZ and Mission Creek strand of the San Andreas fault.

Site Description

Petra Geosciences excavated a paleoseismic trench on the Banning strand at 18th Avenue, in North Palm Springs, California (33.9172°, -116.538°). The purpose of the trench was to determine the precise location of Holocene fault strands for the development of the site as required by the Alquist-Priolo Act of 1972. The lead consultant on the study invited us to conduct a more detailed paleoseismic study on

the open trench. The 4-tier, benched trench was ~250 m long, ~8 m deep, ~9 m wide at the bottom and ~22 m wide at the ground surface. Most of this study is focused on the northern end of the trench where a ~40-m-wide fault zone was exposed in interbedded boulder, cobble, gravel, sand, silt, and clay deposits. The trench was excavated into the flood plain of Mission Creek, a ~5-km-wide, broad alluviated surface that slopes gently to the south (Figure 2, inset).

We observed recent faulting in the northernmost 40 m of the trench. Five fault strands at the north end of the trench exhibited down-to-the-south faulting, whereas the eight to nine prominent fault strands farther south exhibited down-to-the-north separation (Figure 3). The fault geometries and thickened section between them are consistent with a pull-apart basin, which likely formed as a result of a small right-step in the Banning strand evident in publicly available lidar data (Bevis and Hudnut, 2005) (Figure 2).

Within the pull-apart basin, 1- to 20-cm-thick layers of very fine sand, silt and clay were interbedded with coarse sand to granule layers up to 1 m thick. The fine-grained layers were thickest near the center of the pull-apart basin and thinned away from the center. Most of the fine-grained layers either pinched out or gradually became coarse-grained within 16–18 m from the center of the basin. A few fine-grained layers extended all the way to the southern end of the section of the trench that was logged (about 38–40 m from the center of the basin).

South of the fault zone, the trench was dominated by coarse sand and gravel units ~10–30 cm thick; fine-grained layers were absent, and a few layers contained boulders up to 0.5 m in diameter. Overall, the stratigraphy has distinct and abrupt contacts between layers and consistent lateral continuity along the trench wall. Locally, and often near-fault terminations, upper contacts were scoured and overlain by younger deposits. Our ability to follow contacts through the fault zone was locally restricted by two factors: (1) in places the vertical separation (and presumably large lateral separation) produced strong changes in the texture of units across the fault zones and (2) the width of the trench, 9 m at the base and 22 m at the ground surface, made the detailed correlation of strata between the west and east walls of the trench impossible except for a few prominent layers.

Methods

Field Work

Both the east and west walls of the trench had four vertical tiers about ~1.5 m high separated by three horizontal benches (each about ~1.5 m in width). We photographed the entire fault zone and used Structure from Motion photogrammetric techniques to produce a scaled photomosaic that we used to log the trench (Figure 3). Absolute reference frame and scale were determined with a total station survey of a grid of nails placed approximately 2 m apart along the top and base of each tier. The photomosaic provided a base for logging of stratigraphic layers and faulting in the field. The final orthomosaic was rectified using the surveyed nails as control points.

Dating

Thirty-four samples of charcoal, typically collected from fine-grained layers, were radiocarbon dated at the Center for Accelerator Mass Spectrometry at Lawrence Livermore National Laboratory to constrain the ages of the prehistoric earthquake horizons. We used the on-line software OxCal (Bronk Ramsey, 2009) with the IntCal 13 calibration curve (Reimer et al., 2013) to calibrate radiocarbon measurements. The results are listed in Table 1.

A total of 17 samples were collected and dated using post-Infrared Infrared Stimulated Luminescence protocol (p-IR IRSL; Buylaert et al., 2009) at the University of California, Los Angeles Luminescence Lab. The equivalent dose (De) values for individual grains were measured using a modified single-aliquot regenerative (SAR) protocol (Wintle and Murray, 2006) and synthesized into sample De values using conventional age models (Galbraith et al., 1999). Post-IR IRSL225 ages were obtained by dividing De with the geologic dose rate on the DRAC 1.2 online calculator (Durcan et al., 2015). The mean age ± 1σ uncertainty is used to report all luminescence ages (Table 2). Details of the luminescence dating methods used will be provided in Castillo et al (in review, Geosphere).

Recognition of Earthquake Horizons

A central challenge in paleoseismic investigations is to identify horizons that were at the ground surface when (prehistoric) earthquakes ruptured the fault. Upward termination of fault strands is a common type of evidence for an earthquake horizon. However, upward termination of fault strands alone does not always provide a reliable indicator of the stratigraphic position of an earthquake horizon because fault strands with small displacements may not necessarily have ruptured all the way to the ground surface at the time of an event (e.g., Bonilla and Lienkaemper, 1991). Earthquake horizons are considered more reliable if a sedimentary response to the displacement is preserved (e.g., Scharer et al., 2017; Onderdonk et al., 2018). For example, when a graben or uphill-facing fault scarp is formed, it may create a closed depression where water will pond and deposit fine-grained material in the depression. In this configuration, the fault scarp may be preserved and buried by the fine-grained sediments, which generally thin and pinch out at the edges of the depression that formed as a result of vertical separation at the surface. Thus, both the fault strand and the subsequent depositional record provide more robust evidence of the paleoearthquake horizon than simple upward termination alone.

At the 18th Avenue trench, most of the exposed fault strands accommodate a component of down-to-the-north displacement. Given the southward slope of the floodplain of Mission Creek, down-to-the-north displacement on individual fault strands created uphill-facing scarps and ponding of fine-grained sediments. Thinning of fine-grained layers across the scarps that filled fault-bounded depressions provided strong evidence for some of the earthquake horizons at the site.

Event Indicator Quality Ranking

At the 18th Avenue trench, we found evidence for eight paleoearthquake horizons with varying quality. To compare the strength of evidence for the different events, we use a ranking scale to classify each of the indicators based on the quality of structural and sedimentological evidence used to identify the stratigraphic level that was at the ground surface at the time of the event. Each event indicator is given a quality rank on a scale of 0 to 5, with higher numbers representing more reliable evidence (Table 3). Table 3 was developed based on a previously published table in Scharer et al. (2017), with several modifications that tailor the criteria to the 18th Avenue trench. Because of unique considerations related to local geology and fault zone architecture, some site-specific decisions and adjustments were made.

First, it is common for faults that slipped with minor displacement to terminate upwards at different stratigraphic levels because some of the strands did not rupture all the way to the surface (Bonilla and Lienkaemper, 1991; Weldon et al., 2002). Because of this, Scharer et al. (2017) made a distinction between faults with minor versus moderate offset, with the latter being viewed as more likely to have ruptured to the ground surface thus meriting a higher quality ranking. We choose to classify faults as

having “moderate” offset if there is ≥ 5 cm vertical separation, or if the correlation of units across the fault was uncertain due to textural changes, indicating that the lateral slip was reasonably large. Previous studies have documented rupture with up to 20 cm of vertical separation that terminated at different stratigraphic levels during the same prehistoric earthquake (e.g. Weldon et al., 2002; Bonilla and Lienkaemper, 1991). In other studies, earthquakes with displacement of only a few millimeters or less have ruptured to the ground surface (e.g., McGill and Rubin, 1999). Our selection of 5 cm to define “moderate” offset falls between these values.

Second, we adjusted the ranking to take into account the effects of uncertainties in stratigraphic correlation that makes attribution of a specific indicator to a horizon challenging. Specifically, in cases where the upward termination of a fault is not distinct and there are multiple horizons that could reasonably be associated with the upward termination, we assign a quality ranking of 0. If the upward termination is indistinct or unclear, but there is an unfaulted unit that lies below the next higher earthquake horizon, we assign a quality ranking of 1 for minor offset and 2 for moderate offset because this is clearly an event distinct from the next younger event, even if the precise location of the earthquake horizon cannot be determined. It is worth noting that our treatment of upward fault terminations is designed to produce a minimum number of paleoearthquakes. In other words, in cases where a fault terminated below the stratigraphic level of a known earthquake horizon elsewhere in the trench, and if there were no unfaulted layers precluding the fault from extending up to the earthquake horizon, we assumed that fault did extend up to the previously recognized earthquake horizon.

Third, Scharer et al. (2017) made a distinction between folding and thickness changes that are “small” versus “substantial” with the latter being viewed as more likely to have resulted from co-seismic deformation of the ground surface thus meriting a higher quality ranking. We specified thickness changes of 20 cm or more to be “substantial”, thus justifying a ranking of 3, if a causative fault is not clearly identifiable or 4 if a causative fault is identifiable. Our selection of 20 cm reflects typical layer thickness and sharpness of contacts at this site as well as our judgement based on observations in unfaulted portions of the trench that thickness changes and undulations in contacts smaller than this may result from non-tectonic causes.

Stratigraphic Correlation Rankings

Uncertainties in stratigraphic correlation at the 18th Avenue trench led to difficulty in tracing the event horizons across the trench; thus producing additional uncertainty in the event recognition. Because of the broad width of the trench, only four distinctive layers could be confidently correlated between the east and west walls. Even along the same wall of the trench and in the absence of faulting, lateral facies changes, local channel scour, and areas of poorly delineated stratigraphy make it challenging to trace some stratigraphic units over long distances (> 10 m). Most strata could be clearly correlated across faults with minor offset, but stratigraphic correlation is more difficult across a few of the faults with larger amounts of offset.

To address the uncertainty in our stratigraphic correlation of event indicators, we created a stratigraphic correlation ranking table (Table 4). This correlation ranking table requires that a “type locale” be defined for each individual event. We selected the type locale from among the best-ranked event indicators for that specific event (i.e., where the event horizon could be narrowly assigned within a stratigraphic package) and located where it is possible to correlate layers at the type locale with other event indicators. The relative stratigraphic position of each event horizon for each individual indicator is traced

along the trench wall (i.e., within a particular stratigraphic package) to the type section. A stratigraphic correlation rating between 1 and 5 is assigned based on the continuity of the package. A rating of five means an event indicator is easily followed all the way to the type section, confirming it is at the same stratigraphic level as the event horizon at the type section. A rating of one means that the correlation is uncertain enough to create ambiguity as to which event horizon this indicator should be associated. This situation may result from pinch out of marker beds, mismatch or changes in character of units across faults or along section, position of benches, or presence of bioturbated zones. It is worth noting that we attempted to assign each event indicator to an event that also had other indicators, rather than treating each indicator that had an uncertain correlation as a potential independent event. Our method, therefore, is biased for producing the minimal number of events necessary to explain the observations.

Characterizing the Likelihood of Each Event

We qualify the likelihood of a paleoearthquake at each stratigraphic horizon based on the quality and the number of individual event indicators. Following the example of Scharer et al. (2017), we use the terms probable, likely and very likely to denote horizons with increasing probability of representing a paleoearthquake horizon. Also, like Scharer et al. (2017), we use the label probable when the number and quality of event indicators suggest at least a 50% likelihood of a surface-rupturing event at that horizon. At this site, we consider events that have three or more indicators with at least one having a quality rating of 2 or higher to be probable earthquakes. Those with one or two indicators with quality rankings of 3 or higher are considered likely, or very likely, respectively (Table 5). Horizons with isolated, weak evidence that do not meet these criteria are not given an event number. As noted above, our treatment of upward fault terminations and our approach to correlating earthquake indicators are both designed to produce the minimum number of events. It is quite possible that additional events occurred that were not identified due to these approaches. It is also possible that multiple events have occurred at any of the identified horizons if no sedimentation occurred between events.

Site Stratigraphy

The orthorectified, georeferenced and annotated photomosaics for the west and east walls of the trench are shown in Castillo et al. (in review, Geosphere). A simplified representation of the contacts and faults is shown in Figure 3. Strata that could be traced were assigned unit numbers, with unit numbers increasing with stratigraphic depth.

Four correlatable units were used to anchor the stratigraphic numbering of units between the trench walls. The uppermost unit is unit 290, which is a 30-cm-thick silt layer with a distinct thin, brown clay at its base. This unit contains more charcoal fragments than any other unit within the trench. The next lower anchor unit is unit 610. On the east wall, this unit is distinguished by large boulders (~ 0.5 m diameter) within an 0.5- to 1-m-thick layer of coarse sand with pebbles and granules. Boulders this large are not present within any other unit. On the west wall, this unit is sandier and the boulders are smaller (~ 0.25 m), but it is still the coarsest unit on the west wall, and present at a similar depth below the surface. Immediately below unit 610 is unit 620, composed of coarse sand, pebbles and small boulders (~0.25 m diameter) on the west wall and pebbly gravel on the east wall. These two units are separated by a sharp contact. The lowest unit is unit 850, a muddy sand and gravel bed with a sharp upper contact. The unit is brownish in color compared to overlying units that are grayer in color.

All units on the west wall have "W" prefix before the unit number, and those on the east wall have an "E" prefix. Unit numbers between 0–99 were assigned to strata above the E1 earthquake horizon, numbers between 100–199 to strata between the E1 and E2 earthquake horizons, and so on. Except for units 290, 610, 620 and 850, it was impossible to correlate units between the two walls. Thus, units that have the same number but a different prefix (E vs. W) should not be interpreted as correlating across the trench, nor should units with a lower number on one wall necessarily be assumed to be younger than a unit with a higher number on the opposite wall. Uncertainties in correlation of the event horizons were addressed through the correlation ranking system described above (Table 4).

Earthquake Horizons

Specific details about the evidence for each earthquake horizon will be available in Castillo et al. (in review, Geosphere). Figure 4 summarizes the event evidence by illustrating the number of indicators for each event, as well as their quality and stratigraphic correlation rankings. Figures 5-7 show examples of key evidence for most of the events. Applying Table 5, we have one very likely event (E-1), four likely events and three probable events.

Paleoearthquake Ages

Radiocarbon and Luminescence Dating

Layer ages are provided by 34 radiocarbon-dated detrital charcoal samples and 17 sediment samples dated using post-IR IRSL techniques (Tables 1 and 2). All dates are plotted in Figure 8 as a function of stratigraphic depth measured at m24W down to layer W620, and then at m34 for layers older than W620 (Figure 3). These sections were selected because they are within a wide, fault-bounded block with clear stratigraphy and are close to the area where layers are thickest. On Figure 8, all samples from the east wall, and samples from the west wall that are not from the type section, are shown with vertical error bars that indicate the uncertainties in the stratigraphic positions of these samples relative to the type section.

The stratigraphic thickness of 9 meters exposed in the trench was deposited within the past ~7000 years indicating an average depositional rate of ~0.13 cm/yr. Based on the youngest samples at each depth, the sedimentation rate appears to be relatively constant across the section, yet it could be variable from unit to unit given the relatively sparse dating. The longest possible depositional hiatus can be no more than the 1–1.5 ky interval between samples L01 and L17 (~4–5 m depth). There is no clear indication of a hiatus at this time, and a hiatus this long is only possible if deposition stopped immediately after the layer containing L17 formed and the overlying 1 meter of sediment between sample L01 and L17 was deposited very rapidly. Based on texture and bedding, the layers between these two samples could have been deposited in a few depositional events. Episodes of rapid sedimentation may have also occurred, such as between samples L17/L18 and L20/L04/L02, which all have nearly the same age within the 1σ uncertainties, despite spanning about 1.5 m of stratigraphic depth. This depth range is dominated by the two thickest units in the trench, the boulder units 610 and 620, which were likely deposited very rapidly, potentially during the course of one or a few storms. The presence of scouring within some areas (e.g., Figure 2) suggests that parts of the record are locally missing.

Paleoearthquake Model Ages

We used OxCal (Bronk Ramsey, 2009) to estimate the earthquake ages. OxCal uses Bayesian statistics to model posterior ages for the paleoearthquakes based on all chronological constraints such as relative stratigraphic position and layer groups. Dates from the same layer, or from layers that we infer correlate with each other were modeled using the "Phase" command such that relative stratigraphic position within the layer group is not applied (Bronk Ramsey, 2009).

The range of ages for several intervals shown in Figure 8 presents a challenge for constructing a straightforward age model. For example, samples A44 and C10 at 2 m stratigraphic depth have ages that differ by 2000 years, as do samples A18 and A39 at 2.75 m stratigraphic depth. Many studies have shown that it is common for detrital charcoal samples to be older than the age of the layer from which they were collected by an amount that depends on the length of time between when the plant material stopped growing and when the sample was deposited in the location from which it was collected (e.g., Philibosian et al., 2011; McGill et al., 2002; Fumal et al., 2002). Aside from contamination of the sample, the only way for charcoal to underestimate the depositional age of a layer is if it was a root or was brought into the section by bioturbation. We were careful in the field to avoid collecting roots or any charcoal samples from obvious filled burrows or areas lacking clear stratigraphy, which could potentially be bioturbated zones, and we reviewed photographs of the sample locations to evaluate the potential for unrecognized bioturbation at each sample location. To construct our preferred age model, we therefore omitted any charcoal samples with dates that are older than other charcoal or luminescence samples from the same layer or lower layers. In Figure 8, dated samples that are included in our preferred age model are plotted with filled symbols, and those that are excluded are plotted with open symbols.

In total, 29 out of 34 radiocarbon dates have been omitted from our preferred age model, which thus relies heavily on the IRSL ages to constrain the timing of past earthquakes. The omission of this many radiocarbon samples is supported by previous studies that have shown wide ranges of radiocarbon ages for charcoal samples from the same layer (e.g. McGill et al., 2002; Fumal et al., 2002; Philibosian et al., 2011). In the 18th Avenue trench, we also have multiple samples from the same depths with mean radiocarbon ages separated by as much as 2000 years (e.g. samples A44 and C10 at ~2 m depth and A18 and A39 at ~2.6 m depth), suggesting that detrital lag times can be at least 2000 years long on the Mission Creek fan. Fumal et al. (2002) also found lag times of up to ~600-1000 years for charcoal samples from the same layer at a site on the Mission Creek strand at the Thousand Palms site, located about 20 km to the east and which like the 18th Avenue trench has a large source catchment.

One IRSL samples from the east wall (L05) was also excluded from our preferred age model because it was older than most other samples at that stratigraphic depth and it had large uncertainty in its stratigraphic depth relative to the type section on the west wall. The results of the preferred OxCal model are shown in Figure 9 and Table 6.

While it is common practice in paleoseismic studies to omit charcoal samples that are older than other charcoal samples from the same or underlying layers (McGill et al., 2002; Fumal et al., 2002; Philibosian et al., 2011), what may be of concern in this study is that we are also omitting charcoal samples that are older than luminescence samples from the same or underlying layers resulting in an almost exclusive

reliance on the IRSL ages. Therefore, we also created an alternate model that took a different approach based on the observation that the 2000-year lag was based on only two radiocarbon samples. In contrast to the preferred model, the alternate model starts with the assumptions that those samples (A44 and A18) were contaminated by younger material - which can occur during sample collection and preparation - and that radiocarbon samples C10 and A39 were accurate. Samples A44 and A18 were thus removed from the OxCal model, along with sample A31, because it is much older than the five IRSL samples near the base of the section, which we assume are correct based on their reproducibility. To achieve an Oxcal agreement index >50%, samples L16, L06, L07 and L01 were also removed as they are notably younger than both radiocarbon and IRSL samples in the same phase. Given that the IRSL signal measured for these samples is observed not to fade through time, the only reasonable explanation for an apparent IRSL age that is too young is post-depositional mixing. Considering that it is unlikely that post-depositional mixing of grains would systematically shift ages in a way that is stratigraphically consistent, these were not removed in the preferred model. However, this alternative model has some advantage of retaining more of the original radiocarbon data, as it uses 20 of the original 34 radiocarbon and 13 of 17 IRSL samples. In comparison to the preferred model, this approach produces much older earthquake ages for E2-E6 (Figure 10 and Table 6). Although both models are feasible, we rely on the preferred model because it is common for detrital carbon samples to be older than true depositional ages, and the fading tests indicate the IRSL samples are unlikely to be biased too young.

Discussion

Recurrence Intervals

As shown in Figure 4, the overall number of observations and quality rank of event indicators decreases with depth. There are several reasons why the evidence for older events is weaker than for the younger events. First, the older strata are only exposed within a small portion of the fault zone. Second, evidence for older events has been overprinted by younger earthquakes, making interpretation more difficult. Stratigraphic correlation of event indicators to their respective type locales was also a major challenge in this trench at all stratigraphic levels, but was compounded for older events due to increased difficulty in correlating layers across faults in which the cumulative lateral offset in multiple events was large.

The earthquake record at the site includes evidence for five events in the upper three meters, which occurred in the past 2.4–3.3 ka (age range for E5). The mean recurrence interval for these five events on the Banning strand is 490 years (95% range 390-600 years). The individual intervals between each of these five events are very similar to the mean (Figure 10). As noted above, we cannot rule out the possibility that additional earthquakes may have occurred and not been recognized. If the alternate age model is correct, ages for E2 through E6 are 600 to 1800 years older than in the preferred model, producing a mean recurrence interval of 940 years, nearly twice as long as in the preferred model (Figure 10).

Only three events are recognized in the lower 6 meters, during a 2.4–4.7 ky period between events E5 and E8 (Table 6). This suggests that either we are missing events in the lower section, or the recurrence pattern at the 18th Avenue site is variable. We cannot rule out either possibility. However, it is likely that the older part of the earthquake record at this site is incomplete due to limited exposure to make observation of the older stratigraphy. Specifically, the trench does not expose stratigraphy older than E3

north of m16, nor does it expose stratigraphy older than E5 north of m20. Faults with large vertical separations are present in the trench north of m20 yet we had no way to investigate paleoearthquakes older than E5 on these faults. In addition, if there was a 1 to 1.5-ky-long hiatus between the deposition of samples L17 and L01 as permitted in the dating, it is possible that we missed the detection of events during this period.

If the full record of up to eight earthquakes is complete, the average recurrence interval during the past ~7000 years would be about 790 years (95% range 680 to 910 years) (Table 7). If the alternate age model is correct, the average recurrence interval for all eight events would be 770 years (95% range 680 to 870 years) (Table 7).

Comparison to Other Paleoseismic Sites

The mean recurrence interval between the past five surface-rupturing earthquakes at the 18th Avenue site of 490 years (95% range 390-600 years) is longer than the mean recurrence at the three sites on the Coachella section and Mission Creek strand (116–300 years; Philibosian et al., 2011, Sieh and Williams, 1990, Fumal et al., 2002) and is shorter than the mean recurrence interval at the Cabazon trench site on the SGPFZ (~1600 years; Wolff, 2018; Scharer and Yule, 2020). Thus, taking the event record at face value, earthquakes at the 18th Avenue site on the Banning strand occur less frequently than on the Coachella section and Mission Creek strand but more frequently than on the SPGFZ. Please see Castillo et al. (in review, Geosphere) for more detailed analysis of possible prehistoric rupture scenarios.

Implications for Average Slip per Earthquake

The Banning strand of the San Andreas fault has a Holocene slip rate of 2.3–6.2 mm/yr (Gold et al., 2015), based on a fan offset at the Painted Hills site, about 8 km northwest of the 18th Avenue site (Figure 1). Given the elapsed times since the most recent event (945–690 cal BP) and the slip rate at Painted Hills, we calculate the fault could produce slip of 1.6–5.9 m in the next earthquake, using a slip predictable model, and assuming a relatively constant strain release. Using the average recurrence interval of 390–610 years between events E1 and E5 and the slip rate, we estimate that the average slip in these past five events was 1 – 4 m. These estimates of average slip per earthquake are simple in that they do not include uncertainties related to variability in strain release and assume on-fault displacement is comparable at each location. Alternatively, as the fan age at Painted Hills overlaps with the section dated at 18th Avenue, we can infer that the fan has experienced 6-8 earthquakes if all the ruptures spanned the distance between both sites. This would produce an average slip per event of 2.5 – 5 m for the northern Banning strand, assuming the 18th Avenue site record is complete. We note that this range is similar to that predicted from the accrued slip since the most recent earthquake, which may indicate the trench record is complete, or nearly so.

Implications for sediment depositional history

In addition to paleoearthquakes, our study in the Banning strand of the San Andreas fault provides high-resolution sedimentary records with robust chronological controls. This helps to assess the timing and controlling factors of sediment depositional events in this part of southern California. Using the distribution of single-grain K-feldspar post-Infrared Infrared Stimulated Luminescence ages, we examine the timing of the past depositional events in the lower Mission Creek catchment. We analyzed 754 single K-feldspar grains from seventeen samples from the surface to ~8 m depth. Our findings show that the depositional events in the catchment are discrete. At least eight prominent sedimentation events from ~12.0–0.6 ka are identified with recurrence intervals of ~0.5 and ~2.0 ka. The timing of these

depositional events coincides with the periods of high precipitation rates in southern California region. We plan to submit a manuscript to peer-reviewed journal such as Geophysical Research Letters or Journal of Geophysical Research (Saha et al., in prep).

Conclusions

The 18th Avenue site provides the first dated paleoseismic record constructed on the Banning Strand of the SSAF. This 7000-year-long record can now be compared to paleoseismic records on the neighboring strands that make up the complex network of faults in the southern section of the San Andreas Fault. Eight horizons contained evidence of paleoearthquakes based on sedimentological responses to deformation and fault terminations at or below each horizon. These earthquakes are qualified based on the record of deformation and our ability to correlate across this wide trench; E1 is considered Very Likely; E2, E3, E6, and E7 are considered Likely; and E4, E5 and E8 are considered Probable. Based on the stratigraphy, dating uncertainties, and physical limits of the trench exposure, the likelihood of missed events is greatest in the older parts of the section, below E5. The most recent event occurred 945–690 cal BP. The open interval is longer than the average interval between events E1–E5 (390–600 years), but it is shorter than the interval between events E5 to E6 and events E6 to E7. The longer average interval for the entire section (680 to 910 years for events E1-E8) may indicate temporal variations in the rate of strain release on the Banning strand, or it may indicate missing events in the older section of the trench. In the last 1600 years, eight paleoearthquakes are documented at both the Burro Flats and Coachella sites, five on the Mission Creek strand at Thousand Palms, and only two on the Banning and SGPFZ. Given the earthquake ages, a maximum of two earthquakes connecting the Coachella and northern Banning strands are permitted in the last 1600 years, and only one of these events (~600 CE) could have potentially ruptured onto the San Bernardino strand as well. Fewer earthquakes on the Banning strand is consistent with its lower slip rate compared to other sections of the SSAF and would translate to average slip per event of ~1 to 5 m.

REFERENCES

Behr, W.M., Rood, D.H., Fletcher, K.E., Guzman, N., Finkel, R., Hanks, T.C., Hudnut, K.W., Kendrick, K.J., Platt, J.P., Sharp, W.D., Weldon, R.J., and Yule, J.D., 2010, Uncertainties in slip-rate estimates for the Mission Creek strand of the southern San Andreas Fault at Biskra Palms Oasis, southern California: Geological Society of America Bulletin, v. 122, p. 1360-1377, doi:10.1130/B30020.1.

Bevis, M. and Hudnut, K. (2005): B4 Lidar Project: Airborne Laser Swath Mapping (ALSM) survey of the San Andreas Fault (SAF) system of central and southern California, including the Banning segment of the SAF and the San Jacinto fault system. National Center for Airborne Laser Mapping (NCALM), U.S. Geological Survey, the Ohio State University, and the Southern California Integrated GPS Project. Distributed by OpenTopography. https://doi.org/10.5066/F7TQ5ZQ6.

Blisniuk, K. D., Scharer K., Sharp W. D., Burgmann R., Rymer M.J., and Williams P., 2013, New geological slip rate estimates for the Mission Creek strand of the San Andreas fault zone: Southern California Earthquake Center 2013 Annual Meeting, Abstract #032.

Bonilla, M. G., and Lienkaemper, J. J. 1991, Factors affecting the recognition of faults exposed in exploratory trenches. U.S. Geological Survey Bulletin,54.

Brennan, B.J., Lyons, R.G., Phillips, S.W., 1991, Attenuation of alpha particle track dose for spherical grains. Int. J. Radiat. Appl. Instrum. Part D. Nucl. Tracks Radiat. Meas. 18, 249–253.

Bronk Ramsey, C., 2009, Bayesian Analysis of Radiocarbon Dates: Radiocarbon, v. 51, p. 337–360, doi: 10.1017/S0033822200033865.

Buylaert, J., Murray, A., Thomsen, K., Jain, M., 2009, Testing the potential of an elevated temperature IRSL signal from K-feldspar. Radiation Measurements 44, 560–565.

Cardona, J., 2016, Constraining the most recent surface rupture on the Garnet Hill strand, San Andreas Fault, Coachella Valley, California [Master's Thesis]: Northridge, California State University.

Castillo, B., McGill, S.F., Scharer, K.M., Yule, J.D., McPhillips, D., McNeil, J., Saha, S., Brown, N.D., and Moon, S., in review, Prehistoric Earthquakes on the Banning Strand of the San Andreas Fault, North Palm Springs, California: Geosphere.

Durcan J. A., King G. E., Duller GAT. 2015, DRAC: Dose Rate and Age Calculator for trapped charge dating. Quaternary Geochronology 28: 54–61.

Fletcher, K.E.K., Sharp, W.D., Kendrick, K.J., Behr, W.M., Hudnut, K.W., and Hanks, T.C., 2010, 230Th/U dating of a late Pleistocene alluvial fan along the southern San Andreas fault: Geological Society of America Bulletin, v. 122, p. 1347-1359, doi:10.1130/B30018.1.

Fumal T. E., M. J. Rymer, G. G. Seitz, 2002, Timing of Large Earthquakes since A.D. 800 on the Mission Creek Strand of the San Andreas Fault Zone at Thousand Palms Oasis, near Palm Springs, California: Bulletin of the Seismological Society of America, Vol. 92, No. 7, pp. 2841-2860.

Galbraith, R.F., Roberts, R.G., Laslett, G.M., Yoshida, H., Olley, J.M., 1999, Optical dating of single and multiple grains of quartz from Jinmium rock shelter, northern Australia: Part I, experimental design and statistical models. Archaeometry 41, 339–364.

Gold, P. O., Behr, W. M., Rood, D., Kendrick, K., Rockwell, T. K. and Sharp, W. D., 2015, Holocene geologic slip rate for the Banning strand of the southern San Andreas Fault near San Gorgonio Pass: Journal of Geophysical Research: Solid Earth, v. 120, no. 8, p.5639-5663.

Guerin, G., Mercier, N., Nathan, R., Adamiec, C., Lefrais, Y., 2012, On the use of the infinite matrix assumption and associated concepts: a critical review. Radiat. Meas. 47, 778–785.

Heermance, R. V., and Yule, J.D., 2017, Holocene slip rates along the San Andreas fault system in the San Gorgonio Pass and implications for large earthquakes in Southern California. Geophysical Research Letters, Vol. 44, Iss. 11, 5391-5400. DOI:10.1002/2017GL072612.

Huntley, D.J., Baril, M.R., 1997, The K content of the K-feldspars being measured in optical dating or in thermoluminescence dating. Anc. TL 15, 11–13.

Lancaster, J.T., Hayhurst C.A., and Bedrossian, T.L., compliers, 2012, Preliminary Geologic Map of Quaternary Superficial Deposits in Southern California Palm Springs 30' x 60' Quadrangle: California Geological Survey special report 217, Plate 24, scale 1: 100,000.

Lienkaemper, J. J., and Bronk Ramsey, C., 2009, OxCal; versatile tool for developing paleoearthquake chronologies; a primer. Seismological Research Letters, 80(3), 431-434.

Liritzis, I., Stamoulis, K., Papachristodoulou, C., Ioannides, K., 2013, A re-evaluation of radiation dose rate conversion factors. Mediterr. Archaeol. Archaeom. 13, 1–15.

McGill, S.F., Dergham, S., Barton K., Berney-Ficklin, T., Grant, D., Hartling, C., Hobart, K., Minnich, R., Rodriguez, M., Runnerstorm, E., Russell, J., Schmoker, K., Stumfall, M., Townsend, J., and Williams, J., 2002, Paleoseismology of the San Andreas fault at Plunge Creek, near San Bernardino, southern California, Bull. Seismol. Soc. Am. 92, 2803-2840.

McGill, S. F., and Rubin, C. M., 1999, Surficial slip distribution on the central Emerson fault during the June 28, 1992, Landers Earthquake, California. Journal of Geophysical Research, 104, 4811-4833. doi: /10.1029/98JB01556.

Onderdonk, N., McGill, S, Rockwell, T., 2018, A 3700 yr paleoseismic record from the northern San Jacinto fault and implications for joint rupture of the San Jacinto and San Andreas Faults, Geopshere (Boulder, CO), v. 14, iss. 6, 2447-2468, doi: 10.1130/GES01687.1.

Philibosian, B., Fumal, T.E., and Weldon, R.J., 2011, San Andreas Fault earthquake chronology and Lake Cahuilla history at Coachella, California: Bulletin of the Seismological Society of America, v. 101(1), p. 13-38.

Prescott, J. R., and Hutton J.T., 1994, Cosmic ray contributions to dose rates for luminescence and ESR dating: large depths and long-term time variations. Radiation Measurements 23, 497–500.

Reimer, P.J., Bard, E., Bayliss, A., Beck, J.W., Blackwell, P.G., Ramsey, C.B., Buck, C.E., Cheng, H., Edwards, R.L., Friedrich, M., Grootes, P.M., Guilderson, T.P., Haflidason, H., Hajdas, I., et al., 2013, IntCal13 and Marine13 Radiocarbon Age Calibration Curves 0–50,000 Years cal BP: Radiocarbon, v. 55, p. 1869–1887, doi: 10.2458/azu_js_rc.55.16947.

Saha, S., S. Moon, N. D. Brown, E. J. Rhodes, S. F. McGill, B. A. Castillo, K. M. Scharer, D. McPhillips, and D. Yule, in preparation, Sediment depositional history inferred from single-grain luminescence ages in southern California, North America

Scharer, K. M., & Yule, D. A maximum rupture model for the southern San Andreas and San Jacinto Faults California, derived from paleoseismic earthquake ages: observations and limitations. Geophysical Research Letters, e2020GL088532.

Scharer, K., R. Weldon II, Biasi G., Streig A., and Fumal T., 2017, Ground-rupturing earthquakes on the northern Big Bend of the San Andreas Fault, California, 800 A.D. to Present, J. Geophys. Res. Solid Earth, 122, 2193–2218 doi:10.1002/2016JB013606.

Scharer, K., Blisniuk, K., Sharp, W., and Mudd, S. M., 2016, Slip transfer and the growth of the Indio and Edom Hills, southern San Andreas fault. Abstracts with Programs - Geological Society of America, 48(4), Abstract no. 14-3. doi:/10.1130/abs/2016CD-274217.

Stuiver, M., & Polach, H., 1977, Discussion: Reporting of 14C Data. Radiocarbon, 19, 355- 363.

U.S. Geological Survey and California Geological Survey, 2018, Quaternary fault and fold database for the United States, accessed May 2020, from USGS web site: http//earthquake.usgs.gov/hazards/qfaults/.

Weldon, R.J.II, Fumal, T.E., Powers, T.J., Pezzopane, S.K., Scharer, K.M., and Hamilton, J.C., 2002, Structure and earthquake offsets on the San Andreas Faults at the Wrightwood, California paleoseismic site, Bull. Seismo. Soc. Am. 92; no. 7, 2704-2725.

Wintle, A., and Murray, A., 2006, A review of quartz optically stimulated luminescence characteristics and their relevance in single-aliquot regeneration dating protocols. Radiation Measurements 41, 369– 391.

Wolff, L., 2018, 6000-year record of large, infrequent earthquakes on the San Andreas Fault system in San Gorgonio Pass, near Cabazon, California [Master's Thesis]: Northridge, California State University.

Wolff, L. R., and Yule, D., 2014, Reconciling contradicting trench and geomorphologic observations across the San Gorgonio Pass Fault Zone: Southern California Earthquake Center 2014 Annual Meeting, Abstract #282.

Yule, J.D., and Sieh, K., 2003, Complexities of the San Andreas fault near San Gorgonio Pass: Implications for large earthquakes: Journal of Geophysical Research, v. 108, no. B11, ETG 9-1–9-23, doi: 10.1029/2001JB000451.

Yule, J.D., Maloney, S. J., Cummings, L. S., Prentice, C., Ellsworth, W., and Hellweg, P., 2006, Using pollen to constrain the age of the youngest rupture of the San Andreas fault at San Gorgonio Pass. Seismological Research Letters, 77(2), 245.

FIGURES

See next page.

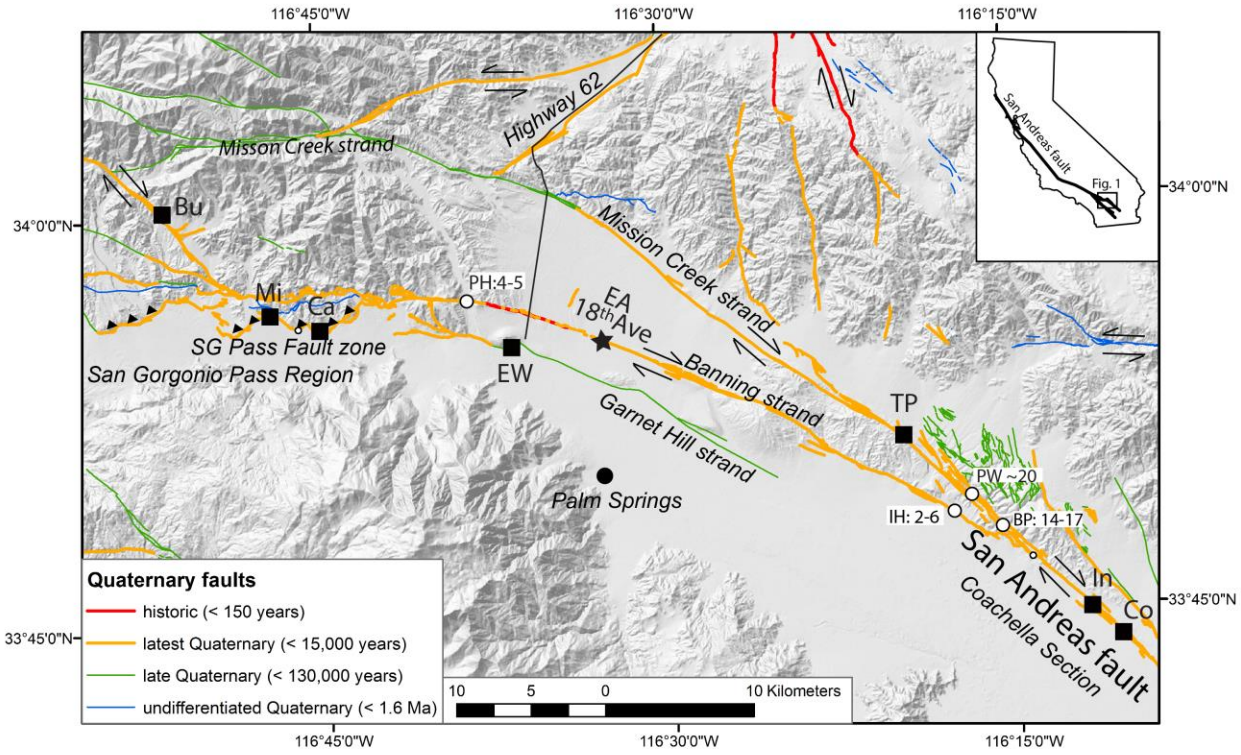

Figure 1*. Quaternary fault map of the greater San Gorgonio Pass region in Southern California. Black star shows the location of the 18th Avenue paleoseismic site on the Banning strand of the SSAF. Black squares mark the locations of other paleoseismic sites mentioned in the text (Co, Coachella, Philibosian et al., 2011; In, Indio, Sieh and Williams, 1990; TP, Thousand Palms, Fumal et al., 2002a; EW, East Whitewater site on the Garnet Hill strand, Cardona, 2016; Ca, Cabazon, Scharer et al., 2013 [abs.]; Wolff et al., 2014; Mi, Millard Canyon, Heermance & Yule, 2017; Bu, Burro Flats, Yule et al., 2007).White circles represents slip rate sites mentioned in the text (PH, Painted Hills, Gold et al., 2015; IH, Indio Hills, Scharer et al., 2016 [abs.]; PW, Pushawalla, Blisniuk et al., 2012; Blisniuk et al., 2013; BP, Biskra Palms, Behr et al., 2010; Fletcher et al., 2010). Quaternary fault locations and recency of movement from USGS (2018).*

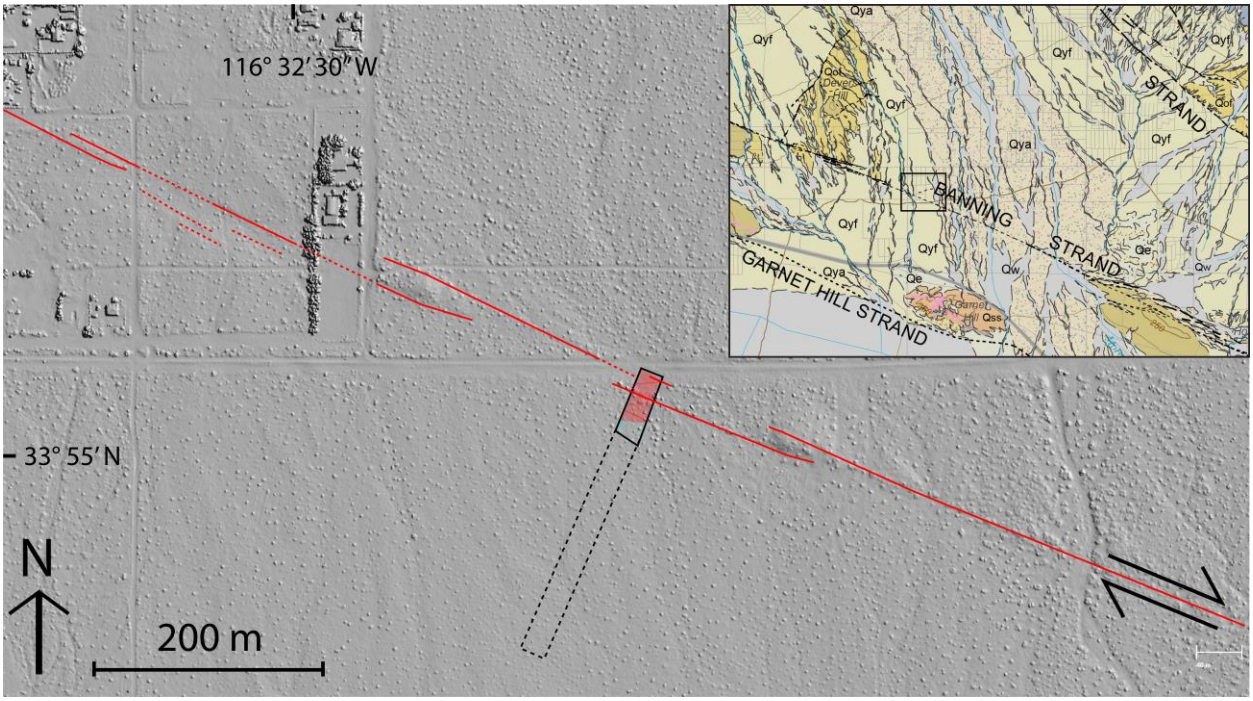

Figure 2. *Lidar hillshade image of the Banning strand (Bevis and Hudnut, 2005). Fault traces (red lines) based on lidar and historical imagery show alternating steps, with left steps consistent with small pop-up structures. Black solid line shows extent of trench shown in Figure 3 and Plate 1. Within the trench, right-stepping faults are consistent with a pull-apart structure. Red polygon outlines extent of faulting observed in trench. No faults were observed in southern ~160 m of trench (black dashed line). Inset map shows setting of the site on alluvial fans and southward-draining channels (Lancaster et al., 2012).*

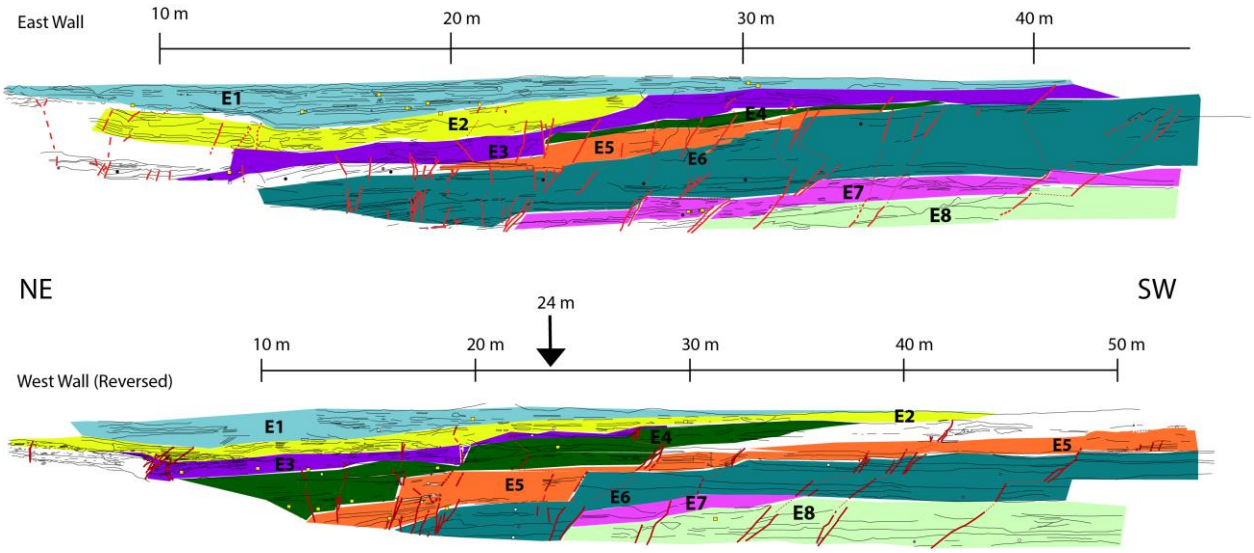

Figure 3. *Simplified trench diagram to highlight thickness changes and extent of sedimentary packages associated with each earthquake. Benched walls are projected onto a single plane, causing some overlap and omission of units. Red, sub-vertical lines are the faults. Dashed thick red lines mark inferred faults in the trench wall. Dashed thin red lines show how faults connect across benches. Arrow on meter 24 on the west wall locates the type section used to construct the stratigraphic age control column; no vertical exaggeration.*

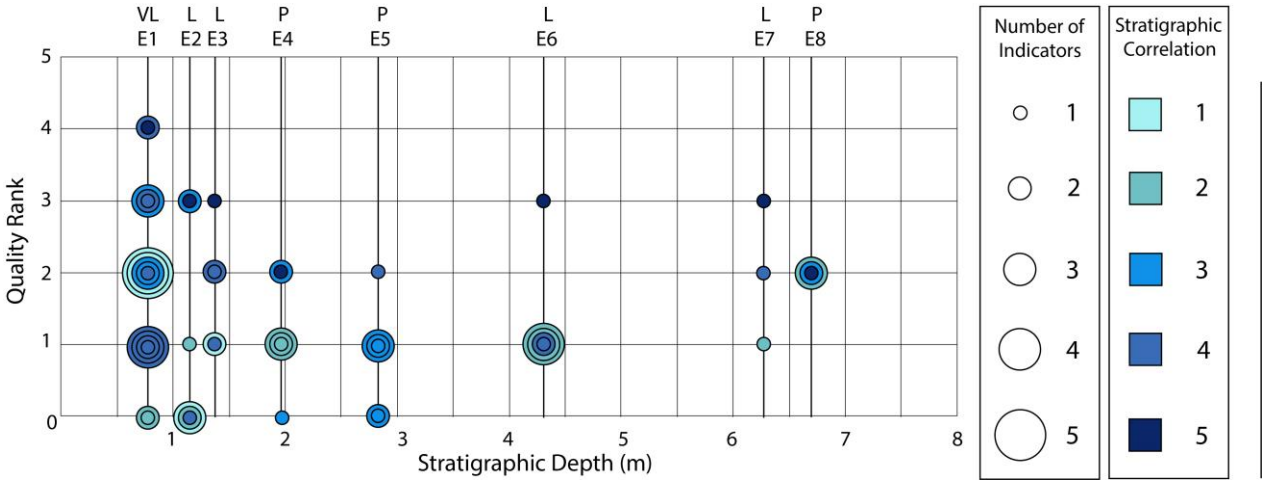

F*igure 4*. *Summary of event Indicators. Eight paleoearthquake horizons were identified in the 18th Avenue trench. Events are arranged according to stratigraphic depth on the horizontal axis, based on the composite stratigraphic column in Figure 13. Vertical axis indicates quality ranking of each indicator, with higher numbers indicating better quality. The diameter of the symbol is scaled by the number of indicators in each rank. For example, earthquake horizon E-1 has 5 individual event indicators with a rank of 2, producing a symbol diameter of 5 Color of the symbols represents the stratigraphic correlation ranking of each event indicator. Indicators with a darker color can be correlated to the type section of the event with greater certainty. For example, of the five rank-2 event indicators for E1, one has a correlation strength of 4, two have a correlation strength of 3, and two have a correlation strength of 1. VL, L, and P indicate the event ranking of very likely, likely, and probable.*

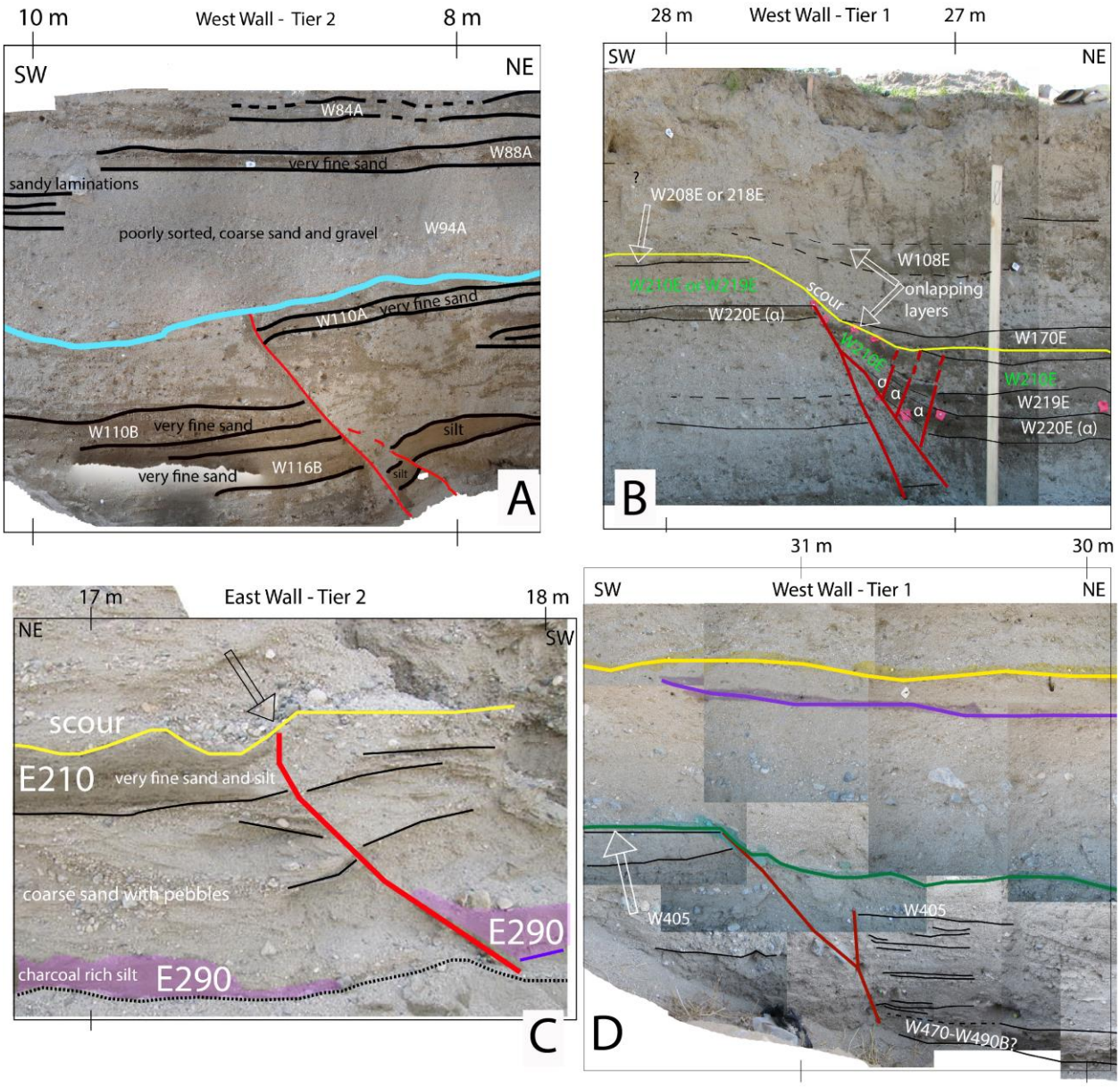

Figure 5. A) *Event 1 evidence. Faulting evidence for event E1 at 8-10 m on Tier 2 of the west wall. A fault terminates sharply at the base of an erosive contact (colored light blue). This fault displays at least moderate offset due to one of the following reasons: 1) There is a very fine sand layer that is visible on both sides of the fault and is labeled as W110A and W110B. If this layer is in fact the same layer, then there is at least 40 cm of vertical separation or 2) If layer W110A is not the same as layer W110B, then correlating layers across the fault is difficult and*

suggests a large amount of lateral offset. A similar relationship is observed at this stratigraphic interval on the east wall.

B) *Event 2 type locale at 26-28 m on Tier 1 of the West Wall. A series of faults terminate upward at the base of the yellow contact (Event 2 horizon). Nature of yellow contact indicates it is an erosional contact showing scour of the ground surface after deposition of W210E, followed by onlap of W170E and younger. This feature has a quality rank of 3.* ***C)*** *Exposures on Tier 2 of East Wall of an indicator for E2. Here, mismatch of units across the fault indicate lateral separation when E210 was at the surface. The fault terminates at the base of an erosive contact (yellow line). This indicator has a quality rank of 3. Purple line shows E3 horizon for context.* ***D)*** *Event 4 Evidence. Type locale for Event 4, at 30-32 m on Tier 1 of the West Wall. Lower part of figure includes photos from a hand-dug, deeper extension of Tier 1 that are not included in Plate 1. Green line spray painted on trench wall highlights the E4 horizon. A fault vertically separates layer W405 and is truncated by an erosional contact (green horizon) that marks the base of a sandy channel. The yellow and purple lines represent earthquake horizons 2 and 3, respectively.*

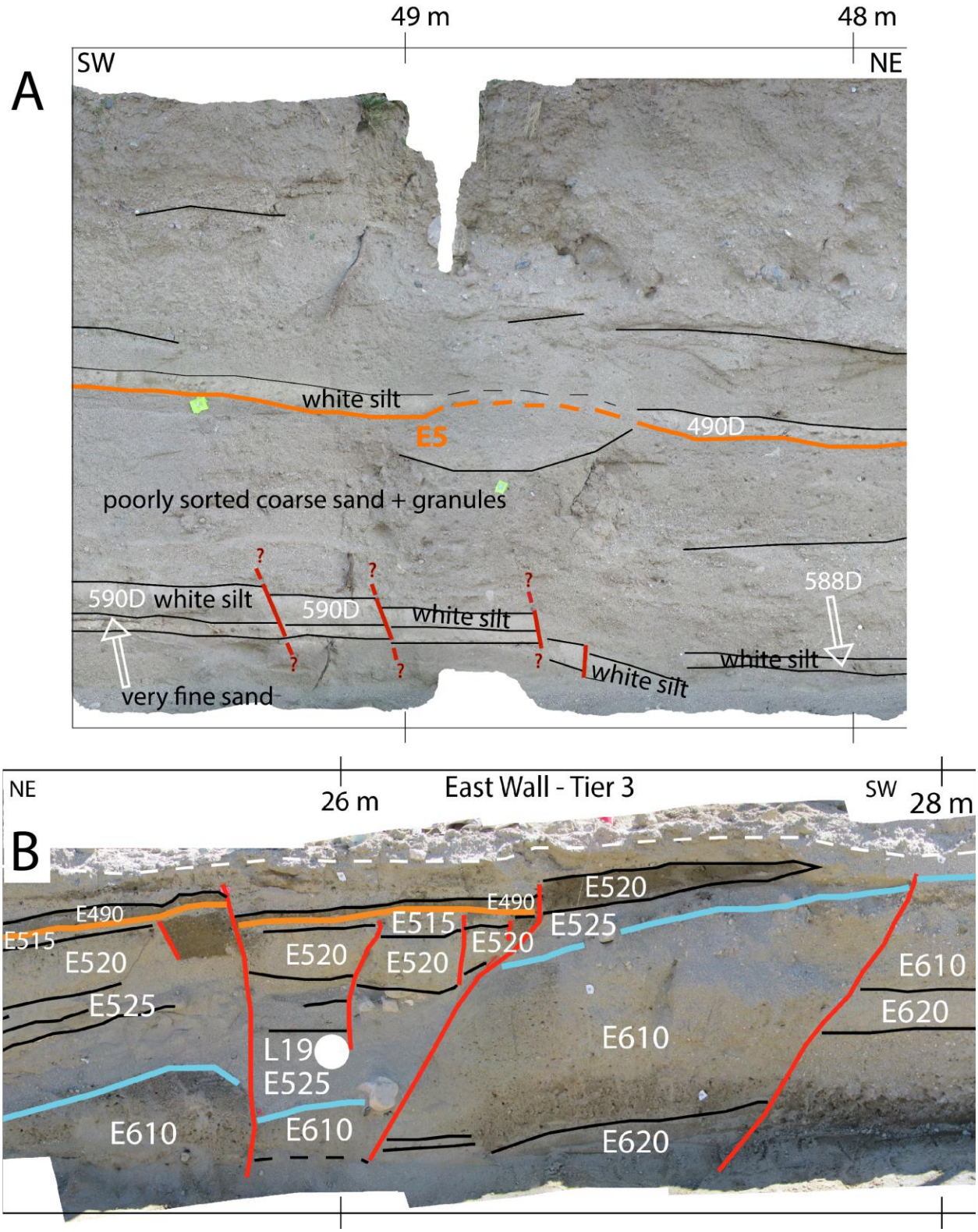
A
49 m
48 m
SW
NE
white silt
E5
490D
poorly sorted coarse sand + granules
590D white silt
590D
white silt
white silt
white silt
588D
very fine sand
B
NE
26 m
East Wall - Tier 3
SW
28 m
E490
E515
E520
E525
E610
L19
E525
E610
E515
E520
E520
E490
E520
E525
E610
E620
E610
E620

Figure 6. A) *Event 5 evidence. Type locale for Event 5, at 48-50 m on Tier 1 of the West Wall. Four faults offset unit 590D but do not appear to offset unit 490D above. The top of the image is the ground surface.*

B) *Event 5 & 6 evidence. Indicators for Events 5 and 6 at 21-27 m on Tier 3 of the East Wall. Several minor faults slipped in E5 and are capped by an unfaulted layer E490. Event E6 is illuminated by layers E520 and E525 which triple in thickness to the northeast (left), suggesting they were deposited within a depression that formed when E610 was at the ground surface. White dashed line marks top of tier 3.*

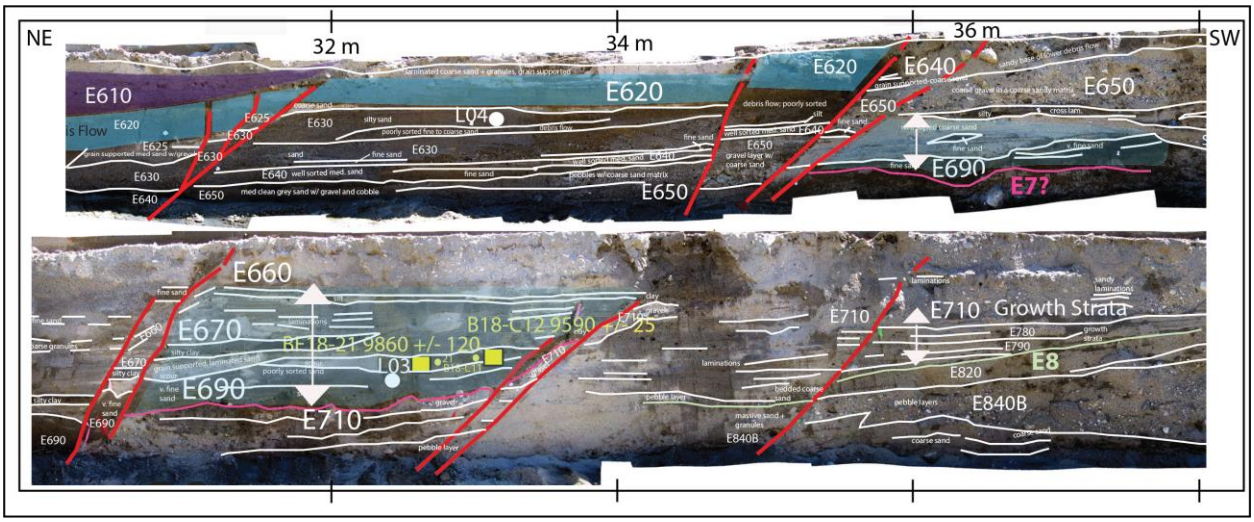

Figure 7: *Event 7 & 8 evidence.Type locale for Event 7 at 34 m on Tier 3 and 4 of the east wall. Layers E660 – E690 thin as they to the southwest (highlighted by light blue). An indicator for Event 8 at 36 m on Tier 4 is shown in the lower photomosaic. Layers E780-E790 thin to the south, filling a depression formed when layer E820 was tilted during Event 8.*

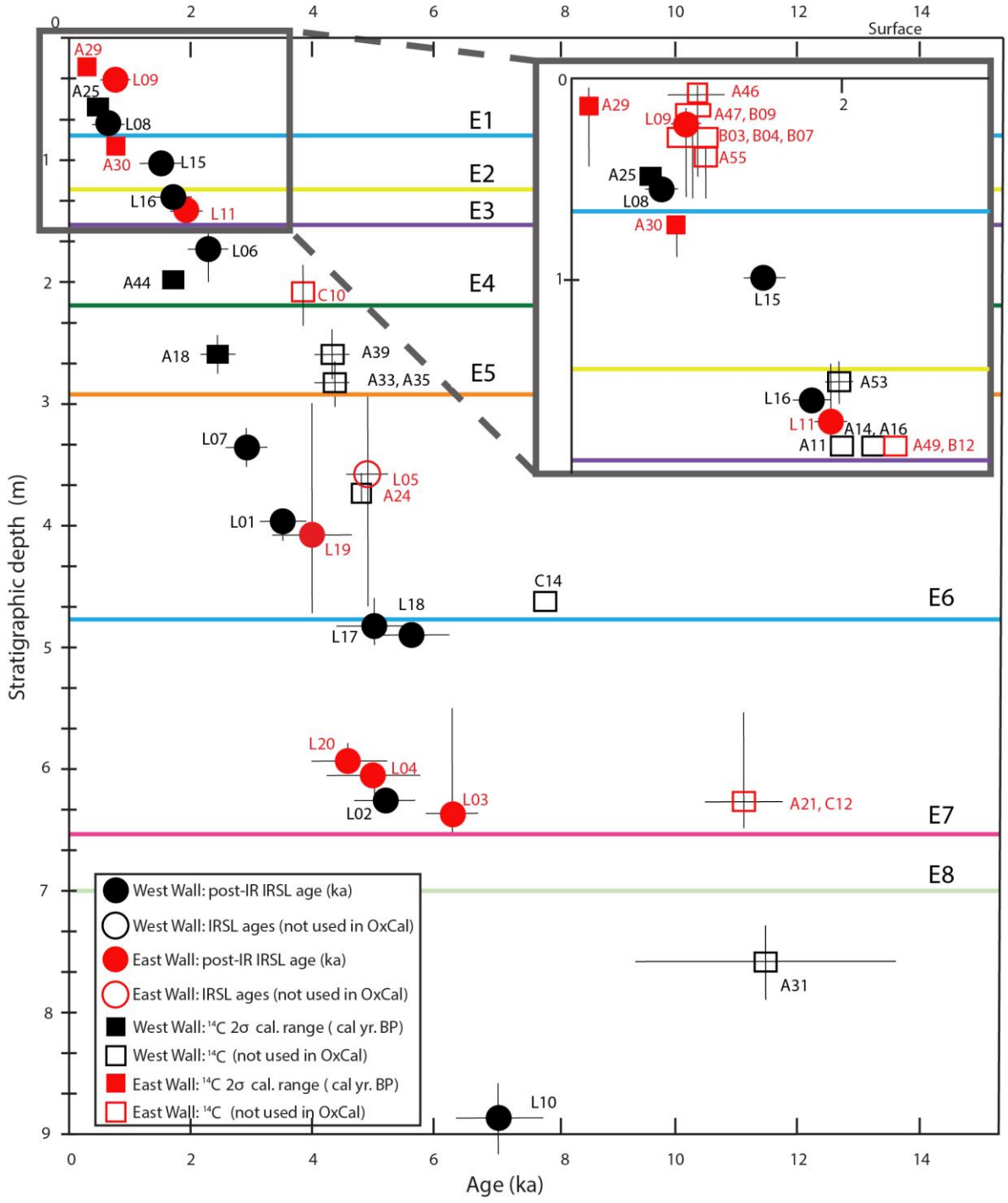

Figure 8. *Calibrated radiocarbon and Post-IR IRSL ages as a function of stratigraphic depth. Stratigraphic depth was measured on the west wall at 24 m (for layers 20 - 620) and at 34 m (for layers 620 - 850). Vertical error bars show uncertainties in correlating sample locations from the*

east wall or from other fault blocks on the west wall with the type section. Solid symbols show ages that were included in our preferred OxCal model; open symbols show samples excluded from that model. Inset shows all ages from the upper 1.6 m.

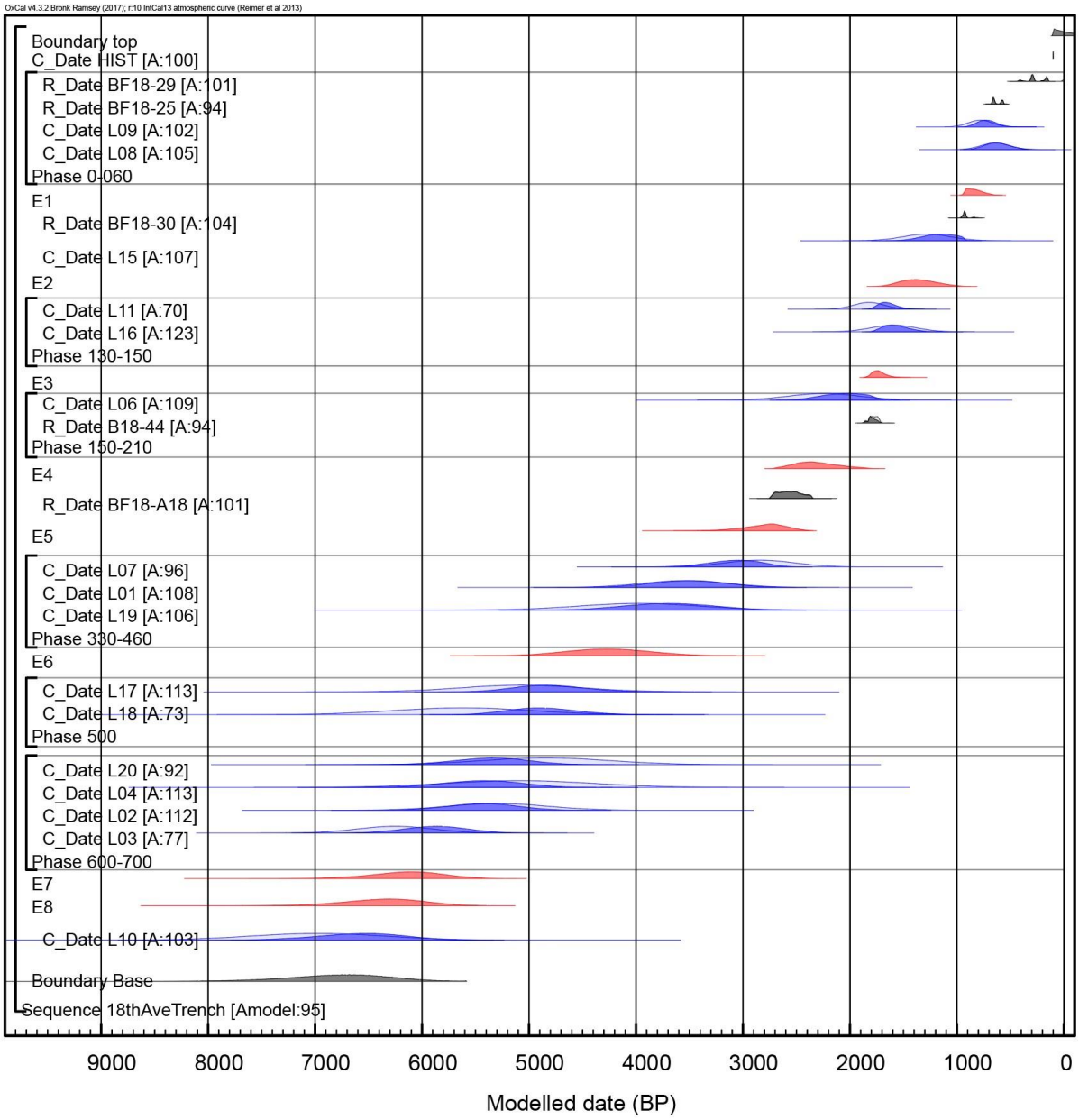

***Figure 9**. Oxcal model to estimate earthquake ages. Ages are plotted as a function of stratigraphic position; blue are IRSL, gray are radiocarbon ages and red are resultant earthquake ages. Brackets indicate samples from same phase (samples from same layer or from layers whose relative stratigraphic position cannot be differentiated). In the Bayesian approach used within OxCal, the ages of samples above and below a given sample are used to reweight the probability density function for that sample so as to yield a set of ages that are stratigraphically consistent with each other as well as being consistent with the a priori (measured) ages of each sample. Pale color shows prior probability density functions (pdfs) obtained for the ages of individual samples. Opaque colors are the posterior pdfs for each sample. This model assumes that charcoal samples provide a maximum age. The model also assumes that IRSL minimum age model methods have correctly estimated the depositional age of the sediment. To achieve an agreement index of >60% (Lienkaemper and Bronk Ramsay, 2009), Twenty-nine radiocarbon samples that are older than stratigraphically lower IRSL or radiocarbon samples were removed. An alternate model that retained more radiocarbon ages is provided in Appendix C; Figure C1 & C2*

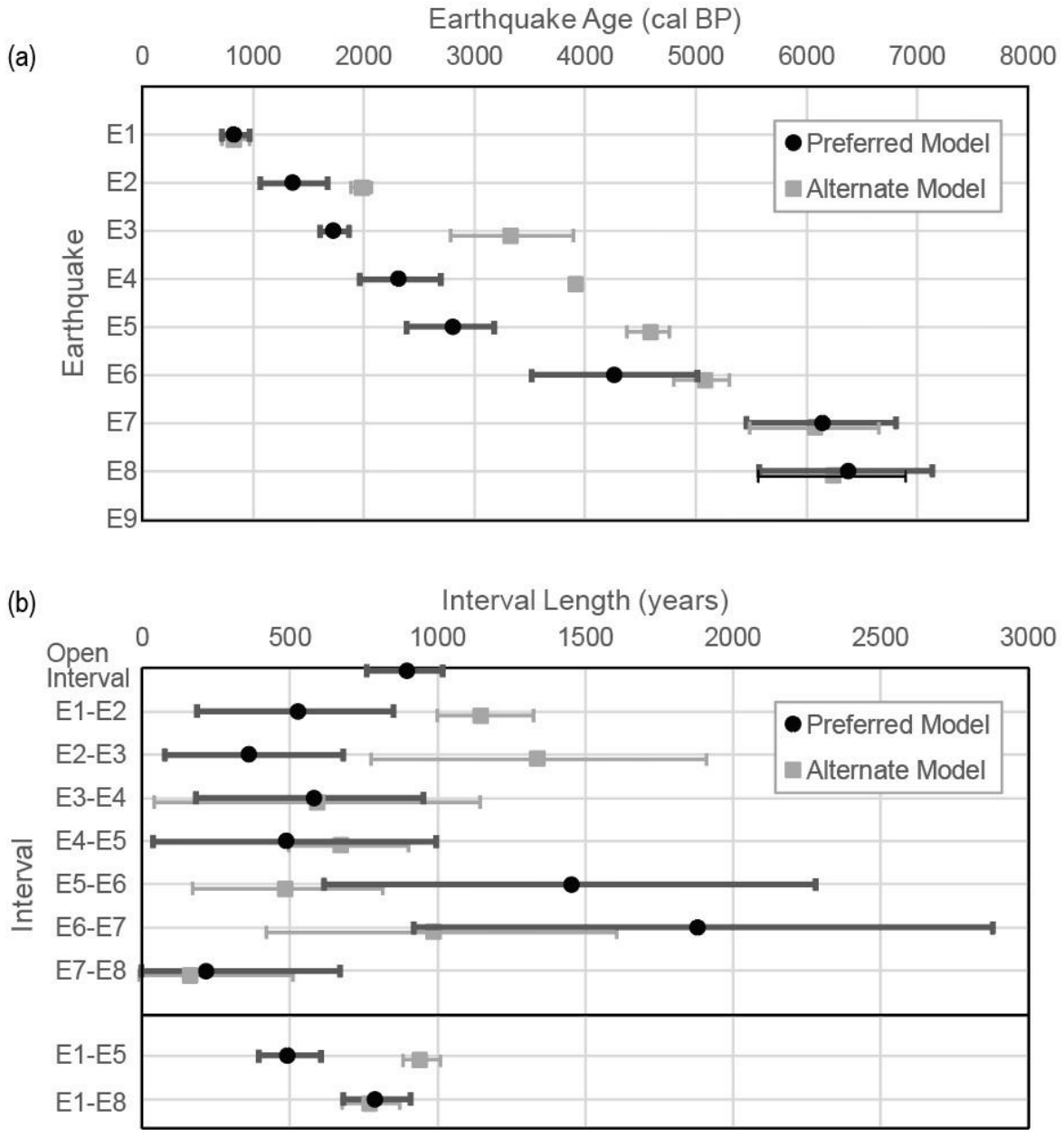

***Figure 10**. Comparison of preferred and alternate earthquake ages (upper) and intervals (lower). The preferred model omits 29 of the radiocarbon ages assuming they reflect significant inheritance due to long transport times. It also assumes the minimum age model accurately resolved the depositional age of the IRSL samples. The alternate model omits five radiocarbon*

samples assuming they were affected by young contamination. The alternate model retains more ages overall and produces older ages for E2 through E5.

TABLES

See next page.

TABLE 1. RADIOCARBON DATES

CAMS #	Original sample name	Strat C. sample name	$\delta^{13}C$	Fraction Modern			$D^{14}C$			^{14}C age			Calibrated ages (BC/AD)			Calibrated Ages (BP)		Sample location	Tier	Meter
													from	to	%	from	to			
176783	BF18-46	A46	-25	0.8731	±	0.0105	-126.9	±	10.5	1090	±	100	693	1155	95.4	1257	795	East wall	1	29.2
176781	BF18-29	A29	-25	0.9708	±	0.0038	-29.2	±	3.8	240	±	35	1522	...	95.4	428	…	East wall	1	17.3
176782	BF18-47	A47	-25	0.8741	±	0.0046	-125.9	±	4.6	1080	±	45	779	1030	95.4	1171	920	East wall	1	29.5
177821	B18-B09	B09	-21.3	0.8853	±	0.0026	-114.7	±	2.6	980	±	25	996	1154	95.4	954	796	East wall	1	9
177818	B18-B07	B07	-24.2	0.8606	±	0.0038	-139.4	±	3.8	1205	±	40	688	945	95.4	1262	1005	East wall	1	19
177819	B18-B03	B03	-22.5	0.8956	±	0.0026	-104.4	±	2.6	885	±	25	1045	1218	95.4	905	732	East wall	1	15
177820	B18-B04	B04	-25.7	1.0921	±	0.0032	92.1	±	3.2	>Modern	±	N.A.†	1896	1904	95.4	54	46	East wall	1	18
176784	BF18-55	A55	-25	0.8602	±	0.0033	-139.8	±	3.3	1210	±	35	689	938	95.4	1261	1012	East wall	1	20.4
176785	BF18-25	A25	-25.5	0.9201	±	0.0027	-79.9	±	2.7	670	±	25	1276	1390	95.4	674	560	West wall	1	20.5
176786	BF18-30	A30	-24.2	0.8832	±	0.0027	-116.8	±	2.7	1000	±	25	987	1149	95.4	963	801	East wall	1	19.3
176787	BF18-53	A53	-25	0.7773	±	0.0043	-222.7	±	4.3	2025	±	45	-165	66	95.4	2115	1884	West wall	1	29
176788	BF18-11	A11	-22.7	0.7258	±	0.0024	-274.2	±	2.4	2575	±	30	-811	-569	95.4	2761	2519	West wall	3	9.8
176789	BF18-14	A14	-24.0	0.7238	±	0.0024	-276.2	±	2.4	2595	±	30	-825	-599	95.4	2775	2549	West wall	3	13
176790	BF18-49	A49	-24.2	0.7265	±	0.0025	-273.5	±	2.5	2565	±	30	-806	-556	95.5	2756	2506	East wall	3	14.5
176791	BF18-16	A16	-25.4	0.7328	±	0.0022	-267.2	±	2.2	2495	±	25	-773	-540	95.4	2723	2490	West wall	3	15
177825	B18-B12	B12	-23.9	0.7334	±	0.0023	-266.6	±	2.3	2490	±	30	-781	-511	95.4	2731	2461	East wall	3	14
176792	BF18-44	A44	-22.6	0.7948	±	0.0021	-205.2	±	2.1	1845	±	25	87	238	95.4	1863	1712	West wall	2	23.5
177826	B18-C10	C10	-25.0	0.6357	±	0.0020	-364.3	±	2.0	3640	±	25	-2130	-1926	95.4	4080	3876	East wall	2	32.5
176793	BF18-18	A20	-25	0.7341	±	0.0051	-265.9	±	5.1	2480	±	60	-777	-416	95.4	2727	2366	West wall	3	20
176794	BF18-39	A39	-25	0.6170	±	0.0026	-383.0	±	2.6	3880	±	35	-2469	-2212	95.4	4419	4162	West wall	4	16
177829	BF18-33	A33	-25	0.6207	±	0.0025	-379.3	±	2.5	3830	±	35	-2457	-2150	95.4	4407	4100	West wall	4	18
177830	BF18-35	A35	-20.6	0.6082	±	0.0019	-391.8	±	1.9	3995	±	30	-2576	-2467	95.4	4526	4417	West wall	4	19.5
177849	BF 18-24	A24	-25	0.5826	±	0.0027	-417.4	±	2.7	4340	±	40	-3086	-2890	95.4	5036	4840	West wall	4	20.5
177833	B18-C14	C14	-24.0	0.4176	±	0.0016	-582.4	±	1.6	7015	±	30	-5987	-5840	95.4	7937	7790	West wall	4	23
176795	BF18-21	A21	-25	0.2932	±	0.0040	-706.8	±	4.0	9860	±	120	-9859	-8855	95.4	11809	10805	East wall	4	31
177834	B18-C12	C12	-22.7	0.3030	±	0.0009	-697.0	±	0.9	9590	±	25	-9151	-8823	95.4	11101	10773	East wall	4	32.5
176796	BF18-31	A31	-25	0.2885	±	0.0299	-711.5	±	29.9	9990	±	840	-11810	-7519	95.4	13760	9469	West wall	4	34
177822	B18-B18	B18	-25	0.7723	±	0.0049	-227.7	±	4.9	2080	±	60	-352	55	95.4	2302	1895	East wall	2	12
177823	B18-C01	C01	-26.7	0.7833	±	0.0023	-216.7	±	2.3	1960	±	25	-38	115	95.4	1988	1835	East wall	1-2	N.A.†
177824	BF18-57	A57	-21.9	0.7244	±	0.0021	-275.6	±	2.1	2590	±	25	-811	-767	95.4	2761	2717	East wall	3	10

177827	B18-B11	B11	-23.7	0.6371	±	0.0022	-362.9	±	2.2	3620	±	30	-2118	-1984	95.4	4068	3934	East wall	3B	14.5
177828	B18-B10	B10	-25	0.6381	±	0.0026	-361.9	±	2.6	3610	±	35	-2120	-1885	95.4	4070	3835	East wall	3B	14.5
177831	B18-B16	B16	-22.0	0.6201	±	0.0019	-379.9	±	1.9	3840	±	25	-2456	-2203	95.4	4406	4153	East wall	3	7
177832	B18-B17	B17	-25	0.6226	±	0.0026	-377.4	±	2.6	3805	±	35	-2435	-2136	95.4	4385	4086	East Wall	3	7

d13C values are the assumed values according to Stuiver and Polach (Radiocarbon, v. 19, p.355, 1977) when given without decimal places. Values measured for the material itself are given with a single decimal place.

The quoted age is in radiocarbon years using the Libby half life of 5568 years and following the conventions of Stuiver and Polach (ibid.).

Radiocarbon concentration is given as fraction Modern, D14C, and conventional radiocarbon age.

Sample preparation backgrounds have been subtracted, based on measurements of samples of 14C-free coal. Backgrounds were scaled relative to sample size.

CAMS# 176783 and 176795 are <30µg C samples.

Error is large on 176796 in part due to the age of sample (nearly two half lives), even though the target was 110µgC

[†]N.A. = not available.

Table 2: Dose-rate information and post-IR IRSL ages

Lab code	Field code	Unit	Depth (m)	K (%) [a]	Th (ppm) [a]	U (ppm) [a]	Measured gamma dose-rate (Gy/ka) [b]	Total dose-rate (Gy/ka)	Equivalent dose (Gy)	Post-IR IRSL age (ka) [c d]
J1284	L01 (BF17-01)	W570	3.8	2.8	19.2	3.28	1.993 ± 0.004	6.011 ± 0.26	21.69 ± 2.2	3.61 ± 0.4
J1285	L02 (BF17-02)	W670	4.9	2.7	18.1	2.56	1.897 ± 0.004	5.466 ± 0.23	29.29 ± 2.15	5.36 ± 0.45
J1286	L03 (BF17-03)	E690	5.1	2.7	16.3	2.65	1.709 ± 0.004	5.037 ± 0.213	31.82 ± 1.16	6.32 ± 0.35
J1287	L04 (BF17-04)	E630	3.5	2.8	15.9	2.57	1.944 ± 0.005	5.487 ± 0.229	28.31 ± 3.6	5.16 ± 0.69
J1288	L05 (BF17-05)	E510	2.6	2.7	21.6	2.78	2.458 ± 0.005	6.372 ± 0.265	31.93 ± 1.76	5.01 ± 0.35
J1289	L06 (BF17-06)	W320	2.9	2.7	17.3	2.46	1.925 ± 0.004	5.69 ± 0.243	13.12 ± 1.78	2.31 ± 0.33
J1290	L07 (BF17-07)	W540C	3.2	2.8	18.7	2.97	1.931 ± 0.004	5.899 ± 0.255	17.19 ± 1.71	2.91 ± 0.32
J1291	L08 (BF17-08)	W82B	0.8	2.7	18.5	2.44	1.891 ± 0.004	5.702 ± 0.242	4.04 ± 0.69	0.71 ± 0.13
J1292	L09 (BF17-09)	E40	0.8	2.9	15.1	2.51	1.716 ± 0.004	5.074 ± 0.214	4.29 ± 0.51	0.85 ± 0.11
J1293	L10 (BF17-10)	W860	6	2.6	19.3	2.46	1.946 ± 0.004	5.542 ± 0.234	39 ± 3.12	7.04 ± 0.64
J1294	L11 (BF17-11)	E260	3	2.8	13.8	2.02	N/A ± N/A	5.212 ± 0.233	9.84 ± 0.57	1.89 ± 0.14
J1394	L15 (BF17-15)	W150E	0.8	2.5	16.1	2.17	1.922 ± 0.005	4.879 ± 0.199	6.59 ± 1.03	1.35 ± 0.22
J1395	L16 (BF17-16)	W220E	1.3	2.8	18.3	2.91	1.874 ± 0.004	5.904 ± 0.256	9.82 ± 1.18	1.66 ± 0.21
J1396	L17 (BF17-17)	W602C	2.4	2.3	16.9	2.73	2.004 ± 0.005	5.517 ± 0.228	28.37 ± 2.84	5.14 ± 0.56
J1397	L18 (BF17-18)	W610	4	2.5	16.3	2.09	1.971 ± 0.005	5.054 ± 0.206	28.74 ± 3.04	5.69 ± 0.64
J1398	L19 (BF17-19)	E525	3.6	2.5	17.5	2.71	2.111 ± 0.005	5.084 ± 0.208	20.55 ± 2.78	4.04 ± 0.57
J1399	L20 (BF17-20)	E620	3.7	2.4	17.4	2.71	1.89 ± 0.005	5.297 ± 0.219	26.03 ± 2.94	4.91 ± 0.59

Location: 33.9174 E, 116.5389 W, 247 m asl.

Grain size used 175-200 μm.

Radionuclide conversion factor after Liritzis et al., 2013; α attenuation factor after Brennan et al., 1991; β attenuation factor after Guerin et al., 2012.

Internal K contents were 12.5±0.5% after Huntley and Baril 1997.

Cosmic dose rates following Prescott and Hutton (1994).

[a] U, Th and K contents derived via ICP-OES with relative uncertainties of 5%.

[b] Gamma dose rate derived from in-situ gamma spectrometry.

[c] Ages are calculated in DRAC-calculator (Durcan et al., 2015).

[d] No fading was observed. Errors reported as 1-sigma

TABLE 3. DESCRIPTION OF EVENT INDICATORS AND ASSOCIATED QUALITY RANKING

Quality	Description
0	Fault tip where upward termination not distinct due to unclear stratigraphy, resulting in uncertainty as to in which event this fault slipped, with no preferred event horizon among the possibilities
	Fault tip with distinct upward termination, but it remains unclear which event the fault is associated with, because the fault terminates upward at a scoured contact that erodes though one or more event horizons
1	Fault with minor offset (<5 cm), even if the upward termination is distinct
	Fault with moderate offset but indistinct upward termination, allowing multiple interpretations for the event horizon during which this fault slipped. Nonetheless, there is reason to prefer association of this indicator with one of these event horizons over the others
	Minor or gradual thickness changes across fault that could simply reflect depositional gradients rather than filling of earthquake produced depression
	Folding amplitude small, and thickness change above horizon of folding is moderate, but stratigraphic location of the lowest unfolded layers is indistinct enough to allow for multiple interpretations for the event horizon during which this folding occurred. Nonetheless, there is reason to prefer one of these event horizons over the others
	Possible fissure which could alternatively be interpreted shear of a massive layer disrupted by multiple fault strands
2	Fault with moderate offset (≥ 5 cm), and indistinct upward termination, but the indicator can still be clearly associated with one event horizon
	Folding amplitude small, and thickness change above horizon of folding is moderate
3	Fault tip with distinct upward termination, moderate offset (≥ 5 cm)
	Folding and thickness changes in layers above folding horizon that are substantial (~20 cm), but folding horizon has no clearly causative fault and (or) the horizon of folding difficult to discern
	Possible fissure for which the fill material does not clearly postdate the inferred event horizon, and both walls of the fissure are faults that have re-ruptured in a younger event
4	Fault tip associated with colluvial wedge or layer thickness changes that reflect modification or erosion of scarp
	Possible fissures for which the fill material does not clearly postdate the inferred event horizon, but a least one wall of the fissure is a fault with a distinct upward termination, which has not re-ruptured in a younger event
	Broad warping and large thickness changes in layer above folding horizon indicate rapid filling of depression, closely related to fault that moved to provide accommodation space
5	Fissures that are clearly filled with the material that postdates inferred event horizon
	Folding and growth strata in which it is clear that the topography was rapidly filled by a single sedimentation event and has a casual fault

Note: modified from Scharer et al., 2017 to reflect the depositional characteristics of the 18th Avenue site.

TABLE 4. DESCRIPTION OF STRATIGRAPHIC CORRELATION RANKINGS

Quality	Description
1	Stratigraphic correlation of one or more event horizons is uncertain enough to create ambiguity as to with which event this indicator should be associated
2	The stratigraphic level of the indicator cannot be physically traced all the way to the type locale, because it crosses more than one fault, bench, or area of poor stratigraphy, leading to a relatively high level of uncertainty, including the possibility that the indicator could correlate with an event other than the proposed event
3	The stratigraphic level of the indicator cannot physically traced all the way to the type locale, because it crosses a fault, a bench, or an area of poor stratigraphy. The correlation of strata is somewhat uncertain, but correlation with the proposed event is much more likely than correlation with any other recognized event. This rating may be applied to an indicator on the opposite wall from type locale for the event, as long as it is not far above or below one of the three layers that have been correlated between the walls (units E/W 290, E/W 610, or E/W 850)
4	The stratigraphic level of the indicator cannot be physically traced all the way to the type locale, because it crosses a fault a bench or an area of poor stratigraphy, but the correlation of strata is fairly certain. This rating may also be applied to an indicator on the opposite wall from type locale for this event, as long as it is not far above or below one of the three layers that have been correlated between the walls (units E/W 290, E/W 610, or E/W 850
5	The stratigraphic level of the indicator can be **physically traced** all the way to the type locale, with no uncertainty in correlation of strata across any faults located between the indicator and type locale. This can only be true for indicators that are on the same wall as the type locale for event

TABLE 5. CRITERIA FOR CHARACTERIZING THE LIKELIHOOD OF EVENTS

Likelyhood	Description
Probable	Three or more individual event indicators, with at least one of 2 or higher; None higher than a quality rank 2
Likely	At least one event indictor with a rank of 3 or higher. Must have 3-5 individual event indicators with at least a rank of 1
Very Likely	Two or more event indicators with a rank of 3 or higher

TABLE 6. EARTHQUAKE AGES

	Preferred Model (cal BP)			Alternate Model (cal BP)		
	mean	95% range		mean	95% range	
E1	830	945	690	830	945	690
E2	1360	1650	1050	1985	2085	1900
E3	1730	1850	1590	3325	3865	2760
E4	2315	2665	1930	3920	3965	3880
E5	2805	3225	2430	4595	4815	4425
E6	4260	5000	3505	5080	5360	4860
E7	6150	6840	5490	6080	6675	5510
E8	6375	7175	5620	6245	6930	5595

Table 7: INTERVALS

	Preferred Model (years)			Alternate Model (years)		
	mean	95% range (cal BP)		mean	95% range (cal BP)	
Open Interval	900	1015	760	N.A.†	N.A.†	N.A.†
E1-E2	530	185	850	1150	1000	1325
E2-E3	365	75	680	1340	775	1910
E3-E4	585	180	950	595	40	1145
E4-E5	490	35	995	675	495	900
E5-E6	1455	615	2280	485	170	815
E6-E7	1885	920	2880	990	420	1605
E7-E8	220	0	670	165	0	510
E1-E5	490	390	600	940	880	1010
E1-E8	790	680	910	770	680	870

†N.A. = not available.

PROJECT DATA

The project data include annotated photomosaics of the trench walls, showing evidence for the paleoearthquakes, and radiocarbon and Infra-red Stimulated Luminescence (IRSL) ages that constrain the ages of these earthquakes. All of these are included within a peer-reviewed article that will be published in the journal *Geosphere*. The article has been reviewed and revised and will be resubmitted to *Geosphere* in early October 2020. The article includes appendices describing in detail each piece of evidence for each paleoseismic event and plots showing the IRSL data for each dated sample. Plate 1 provides the annotated photomosaics of both trench walls, and individual figures within the paper document the best evidence for each paleoseismic event.

BIBLIOGRAPHY OF PUBLICATIONS RESULTING FROM THE WORK PERFORMED UNDER THIS AWARD

Castillo, B., McGill, S.F., Scharer, K.M., Yule, J.D., McPhillips, D., McNeil, J., Saha, S., Brown, N.D., and Moon, S., in review, Prehistoric Earthquakes on the Banning Strand of the San Andreas Fault, North Palm Springs, California: Geosphere.

Castillo, B., McGill, S.F., Scharer, K.M., Yule, J.D., McPhillips, D., McNeil, J., Saha, S., Brown, N.D., and Moon, S., 2020, Ages of Prehistoric Earthquakes on the Banning Strand of the San Andreas Fault, near North Palm Springs, California: Geological Society of America Cordilleran Annual Section Meeting, Paper 17-2, Geological Society of America Abstracts with Programs. Vol. 52, No. 4, doi: 10.1130/abs/2020CD-346897

Castillo, B., McGill, S.F., Scharer, K.M., Yule, J.D., McPhillips, D., McNeil, J., Saha, S., Brown, N.D., and Moon, S., 2020, Ages of Prehistoric Earthquakes on the Banning Strand of the San Andreas Fault, near North Palm Springs, California: Southern California Earthquake Center 2019 Annual Meeting, poster #134.

Castillo, B., McGill, S.F., Scharer, K.M., Yule, J.D., McPhillips, D., McNeil, 2018, Preliminary ages of Prehistoric Earthquakes on the Banning Strand of the San Andreas Fault, near North Palm Springs, California: American Geophysical Union, Fall 2018 meeting, Paper S41D-0581.

Castillo, B., McGill, S.F., Scharer, K.M., Yule, J.D., McPhillips, D., McNeil, J., 2018, Preliminary ages of Prehistoric Earthquakes on the Banning Strand of the San Andreas Fault, near North Palm Springs, California: Geological Society of America Annual Meeting (Indianapolis, IN), Paper Number 195-24, Geological Society of America Abstracts with Programs. Vol. 50, No. 6, doi: 10.1130/abs/2018AM-321086

Castillo, B., McGill, S.F., Scharer, K.M., Yule, J.D., McPhillips, D., McNeil, J. and Pace, A., 2018, Preliminary ages of Prehistoric Earthquakes on the Banning Strand of the San Andreas Fault, near North Palm Springs, California: Southern California Earthquake Center 2019 Annual Meeting, poster #268.

Castillo, B., McGill, S.F., Scharer, K.M., Yule, J.D., McPhillips, D., McNeil, 2018, Preliminary ages of Prehistoric Earthquakes on the Banning Strand of the San Andreas Fault, near North Palm Springs, California: Geological Society of America Rocky Mountain/Cordilleran Annual Section

Meeting, Paper 4-4, Geological Society of America Abstracts with Programs. Vol. 50, No. 5, doi: 10.1130/abs/2018RM-313451

Saha, S., S. Moon, N. Brown, and E. Rhodes, 2019, Inferring sediment dynamics using single-grain feldspar post-IR IRSL luminescence dating in southern California, North America: American Geophysical Union, Fall 2019 meeting, Paper GC13A-06.

Saha, S., S. Moon, N. D. Brown, E. J. Rhodes, S. F. McGill, B. A. Castillo, K. M. Scharer, D. McPhillips, and D. Yule, 2019, Influence of sediment dynamics and alluvial fan formation on paleoseismic studies in southern California, North America: Southern California Earthquake Center 2019 Annual Meeting, poster #129.

Saha, S., S. Moon, N. D. Brown, E. J. Rhodes, S. F. McGill, B. A. Castillo, K. M. Scharer, D. McPhillips, and D. Yule, in preparation, Sediment depositional history inferred from single-grain luminescence ages in southern California, North America

COPIES OF PUBLICATIONS RESULTING FROM THE WORK PERFORMED UNDER THIS AWARD

See next page.

AGU 100 ADVANCING EARTH AND SPACE SCIENCE | FALL MEETING
Washington, D.C. | 10–14 Dec 2018

S41D-0581: Preliminary ages of prehistoric earthquakes on the Banning Strand of the San Andreas Fault, near North Palm Springs, California

Thursday, 13 December 2018
08:00 - 12:20
Walter E Washington Convention Center - Hall A-C (Poster Hall)

The southernmost section of the San Andreas Fault (SAF) is the only section of that fault that has not ruptured historically. It is not known whether this long quiescent period reflects a long average recurrence interval for this portion of the fault, or whether the current interseismic interval is longer than average. Near Indio, the SAF splits into 3 strands; limited paleoseismic work has been conducted on the Mission Creek and Garnet Hill strands and the Banning strand has no available age control for any surface-rupturing, prehistoric earthquakes. We studied a paleoseismic trench that was excavated across the Banning strand by Petra Geosciences (33.9172°, -116.538°). The trench displayed a ~30 m wide fault zone in interbedded alluvial sand and gravel, coarse-grained debris flow deposits, and clay/silt deposits. We were able to document evidence for nine prehistoric earthquakes, with the events higher in the section having stronger evidence than those deeper in the section. The most recent event occurred sometime before deposition of a detrital charcoal sample that has a calibrated date range of 674 - 560 cal BP, and after sample with an age of 963 - 801 cal BP. Three earthquakes have occurred since ~1.8 ka, four earthquakes since ~2.7 ka, and five earthquakes have likely occurred since 5.0 ka. These event rates assume the section is complete and there are no missed events. Three charcoal samples located at the base of the trench had calibrated ages of 10.7 to 11.8 ka. All dates are based on detrital charcoal, so we use the youngest dated sample to constrain the age of each layer. Dates from luminescence samples are pending and will help to address the degree of inherited charcoal and place additional age constraints on individual events. From existing dates, we calculate a maximum average interval of 720 yrs based on three complete earthquake cycles between earthquakes 1 and 4 or a minimum average interval of 330 yrs based on limiting ages for earthquakes 1 and 5. This makes the average interval equal to or less than the current open interval on the Banning strand. Compared to nearby paleoseismic sites, the Banning appears to be intermediate; shorter intervals than published for the San Gorgonio Pass Thrust (~1000 yrs) but longer than the Mission Creek (~215 yrs) and Coachella sections (~220 yrs) of the SAF.

Authors

Bryan Adriel Castillo
California State University San Bernardino

Doug Yule
California State University Northridge

Sally F McGill
California State Univ

Devin McPhillips
U.S. Geological Survey

Katherine M Scharer
U.S. Geologic Survey

James McNeil
California State University Northridge

Find Similar

View Related Events

Day: Thursday, 13 December 2018

GSA Annual Meeting in Indianapolis, Indiana, USA - 2018

Paper No. 195-24
Presentation Time: 9:00 AM-6:30 PM

PRELIMINARY AGES OF PREHISTORIC EARTHQUAKES ON THE BANNING STRAND OF THE SAN ANDREAS FAULT, NEAR NORTH PALM SPRINGS, CALIFORNIA

CASTILLO, Bryan[1], MCGILL, Sally[1], SCHARER, Katherine M.[2], YULE, Doug[3], MCPHILLIPS, Devin[2] and MCNEIL, James[3], (1)Geological Sciences, California State University, San Bernardino, 5500 University Parkway, San Bernardino, CA 92407, (2)U.S. Geological Survey, Earthquake Science Center, 525 South Wilson Ave, Pasadena, CA 91106, (3)Department of Geological Sciences, California State University Northridge, 18111 Nordhoff Street, Northridge, CA 91330

The southernmost section of the San Andreas Fault (SAF) is the only section of the fault that has not ruptured in the last 200 years. It is not known whether this long quiescent period reflects a long average recurrence interval for this portion of the fault, or whether the current interseismic interval is longer than average. Near Indio, the SAF splits into 3 strands; limited paleoseismic work has been conducted on the Mission Creek and Garnet Hill strands and the Banning strand has no available age control for any surface-rupturing, prehistoric earthquakes. We studied a paleoseismic trench that was excavated across the Banning strand by Petra Geosciences (33.9172°, -116.538°). The trench exposed a ~30 m wide fault zone in interbedded alluvial sand and gravel, coarse-grained debris flow deposits, and clay/silt deposits. We documented evidence for eight prehistoric earthquakes, and we note that evidence for the events higher in the section is stronger than the evidence for those that are deeper in the section. Based on the age of two charcoal samples that bracket the most recent event (MRE), it occurred sometime between 560 and 960 cal. BP. We interpret that three earthquakes have occurred since ~1.8 ka, four earthquakes since ~2.7 ka, and five earthquakes have likely occurred since 5.0 ka. These event rates assume the stratigraphic section is complete and there are no missed events. Three charcoal samples located at the base of the trench have calibrated ages of 10.7 to 11.8 ka. All dated samples are detrital charcoal, so we use the youngest dated sample to estimate the age of each layer. Dates from luminescence samples are pending and will help to address the degree of inherited charcoal and place additional age constraints on individual events. Using our existing radiocarbon ages, we calculate a maximum average interval of 720 yrs based on three complete earthquake cycles between earthquakes 1 and 4 or a minimum average interval of 330 yrs based on limiting ages for earthquakes 1 and 5. This makes the average interval equivalent to or less than the elapsed time since the MRE on the Banning strand. The average recurrence interval for the Banning section of the SAF appears to be intermediate between that for the San Gorgonio Pass thrust fault (˜1000 years) and that for the Mission Creek and Coachella sections (˜215 and ˜220 years, respectively).

Session No. 195--Booth# 360

D60. Structural Geology (Posters)
Tuesday, 6 November 2018: 9:00 AM-6:30 PM

Halls J-K (Indiana Convention Center)

Geological Society of America *Abstracts with Programs.* Vol. 50, No. 6
doi: 10.1130/abs/2018AM-321086

Back to: D60. Structural Geology (Posters)

<< Previous Abstract | Next Abstract >>

Joint 70th Rocky Mountain Annual Section / 114th Cordilleran Annual Section Meeting - 2018

Paper No. 4-4
Presentation Time: 11:25 AM

PRELIMINARY AGES OF PREHISTORIC EARTHQUAKES ON THE BANNING STRAND OF THE SAN ANDREAS FAULT, NEAR NORTH PALM SPRINGS, CALIFORNIA

CASTILLO, Bryan[1], MCGILL, Sally[1], SCHARER, Kate[2], YULE, Doug[3], MCNEIL, James[3] and MCPHILLIPS, Devin[2], (1)Geological Sciences, California State University, San Bernardino, 5500 University Parkway, San Bernardino, CA 92407, (2)U.S. Geological Survey, 525 South Wilson Ave, Pasadena, CA 91106, (3)Department of Geological Sciences, California State University Northridge, 18111 Nordhoff Street, Northridge, CA 91330

The southernmost section of the San Andreas Fault (SAF) is the only section of that fault that has not ruptured historically. It is not known whether this long quiescent period reflects a long average recurrence interval for this portion of the fault, or whether the current interseismic interval is longer than average. Near Indio, the SAF splits into 3 strands; limited paleoseismic work has been conducted on the Mission Creek and Garnet Hill strands and the Banning strand has no available age control for any surface-rupturing, prehistoric earthquakes. We studied a paleoseismic trench that was excavated across the Banning strand by Petra Geosciences (33.9172°, -116.538°). The trench displayed a ~30 m wide fault zone in interbedded alluvial sand and gravel, coarse-grained debris flow deposits, and clay/silt deposits. We were able to document clear evidence for five prehistoric earthquakes and possible evidence for four additional events. The most recent event occurred sometime before deposition of a detrital charcoal sample that has a date range of 746-626 cal BP, and after sample with an age of 1119-864 cal BP. At least 3-4 earthquakes have occurred since a ~2.7 ka. At great depths, we document two events with strong evidence and two other possible event horizons with weak evidence. Two charcoal samples located at the base of the trench had calibrated ages of ~11.4 ka. All dates are based on detrital charcoal, so we use the youngest dated sample to constrain the age of each layer. From existing dates, we calculate a maximum average interval of 720 yrs based on three complete earthquake cycles between earthquakes 1 and 4 or a minimum average interval of 330 yrs based on limiting ages for earthquakes 1 and 5. This makes the average interval equal to or less than the current open interval on the Banning strand. Compared to nearby paleoseismic sites, the Banning strand appears to be intermediate; shorter intervals than published for the San Gorgonio Pass Thrust (~1000 yrs) but longer than the Mission Creek (~215 yrs) and Coachella sections (~220 yrs) of the SAF.

Session No. 4

T1. Miocene to Recent Evolution of the Lower Colorado River Corridor and the Northern Gulf of California I
Tuesday, 15 May 2018: 10:20 AM-12:05 PM

Coconino Room (DoubleTree by Hilton)

Geological Society of America *Abstracts with Programs.* Vol. 50, No. 5
doi: 10.1130/abs/2018RM-313451

Back to: T1. Miocene to Recent Evolution of the Lower Colorado River Corridor and the Northern Gulf of California I

<< Previous Abstract | *Next Abstract*

Cordilleran Section - 116th Annual Meeting - 2020

Paper No. 17-2
Presentation Time: 8:20 AM

AGES OF PREHISTORIC EARTHQUAKES ON THE BANNING STRAND OF THE SAN ANDREAS FAULT, NEAR NORTH PALM SPRINGS, CALIFORNIA

CASTILLO, Bryan[1], MCGILL, Sally[1], SCHARER, Katherine M.[2], YULE, Doug[3], MCPHILLIPS, Devin[2], MCNEIL, James[3], SAHA, Sourav[4], BROWN, Nathan D.[4] and MOON, Seulgi[4], (1)Geological Sciences, California State University, San Bernardino, 5500 University Parkway, San Bernardino, CA 92407, (2)U.S. Geological Survey, Earthquake Science Center, 525 South Wilson Ave, Pasadena, CA 91106, (3)Geological Sciences, Cal State University Northridge, Northridge, CA 91330, (4)Department of Earth, Planetary, and Space Science, University of California, Los Angeles, 595 Charles Young Dr. East, Los Angeles, CA 90095

The southernmost section of the San Andreas Fault (SAF) is the only section of that fault that has not ruptured in the last 200 years. It is not known whether this long quiescent period reflects a long average recurrence interval for this portion of the fault or whether the current interseismic interval is longer than average. Near Indio, the SAF splits into 3 strands; limited paleoseismic work has been conducted on the Mission Creek and Garnet Hill strands and the Banning strand has no available age control for any surface-rupturing prehistoric earthquakes. We studied a paleoseismic trench that was excavated across the Banning strand by Petra Geosciences (33.9172°, -116.538°). The trench exposed a ~40 m-wide fault zone in interbedded alluvial sand and gravel, coarse-grained debris flow deposits, and clay-silt deposits. We present the first paleoseismic record for the Banning strand of the southern SAF. The most recent event occurred between 730 and 950 cal BP, potentially coincident with rupture of the San Gorgonio Pass Fault Zone. We interpret that five earthquakes have occurred since 3.3-2.5 ka and eight earthquakes have likely occurred since 7.1-5.7 ka. It is possible that additional events may have occurred without being recognized, especially in the deeper section the stratigraphy, which was not fully exposed across the fault zone. We calculate an average recurrence interval of 380 - 640 yrs based on four complete earthquake cycles between earthquakes 1 and 5. The average recurrence interval is thus equivalent to or less than the elapsed time since the most recent event on the Banning strand. The recurrence interval is similar to that of the San Gorgonio Pass Fault Zone (450-1850 years) but longer than that for the Mission Creek strand (~220 years).

Session No. 17

D7. Paleoearthquake Records and Slip Rates Across the Southern California Plate Boundary
Wednesday, 13 May 2020: 8:00 AM-12:00 PM

Madera Room (The Westin Pasadena)

Geological Society of America *Abstracts with Programs.* Vol. 52, No. 4
doi: 10.1130/abs/2020CD-346897

Back to: D7. Paleoearthquake Records and Slip Rates Across the Southern California Plate Boundary

<< Previous Abstract | Next Abstract >>

Preliminary ages of prehistoric earthquakes on the Banning Strand of the San Andreas Fault, near North Palm Springs, California

Bryan A. Castillo, Sally F. McGill, Katherine M. Scharer, Doug Yule, Devin McPhillips, James C. McNeil, & Alan Pace

Submitted August 13, 2018, SCEC Contribution #8431, 2018 SCEC Annual Meeting Poster #268

The southernmost section of the San Andreas Fault (SAF) is the only section of the fault that has not ruptured in the last 200 years. It is not known whether this long quiescent period reflects a long average recurrence interval for this portion of the fault, or whether the current interseismic interval is longer than average. Near Indio, the SAF splits into 3 strands; limited paleoseismic work has been conducted on the Mission Creek and Garnet Hill strands and the Banning strand has no available age control for any surface-rupturing, prehistoric earthquakes. We studied a paleoseismic trench that was excavated across the Banning strand by Petra Geosciences (33.9172°, -116.538°). The trench exposed a ~30 m wide fault zone in interbedded alluvial sand and gravel, coarse-grained debris flow deposits, and clay/silt deposits. We documented evidence for eight prehistoric earthquakes, and we note that evidence for the events higher in the section is stronger than the evidence for those that are deeper in the section. Based on the age of two charcoal samples that bracket the most recent event (MRE), it occurred sometime between 560 and 960 cal. BP. We interpret that three earthquakes have occurred since ~1.8 ka, four earthquakes since ~2.7 ka, and five earthquakes have likely occurred since 5.0 ka. These event rates assume the stratigraphic section is complete and there are no missed events. Three charcoal samples located at the base of the trench have calibrated ages of 10.7 to 11.8 ka. All dated samples are detrital charcoal, so we use the youngest dated sample to estimate the age of each layer. Dates from luminescence samples are pending and will help to address the degree of inherited charcoal and place additional age constraints on individual events. Using our existing radiocarbon ages, we calculate a maximum average interval of 720 yrs based on three complete earthquake cycles between earthquakes 1 and 4 or a minimum average interval of 330 yrs based on limiting ages for earthquakes 1 and 5. This makes the average interval equivalent to or less than the elapsed time since the MRE on the Banning strand. The average recurrence interval for the Banning section of the SAF appears to be intermediate between that for the San Gorgonio Pass thrust fault (˜1000 years) and that for the Mission Creek and Coachella sections (˜215 and ˜220 years, respectively).

Key Words
Paleoseismology, San Andreas Fault, Banning strand

Citation
Castillo, B. A., McGill, S. F., Scharer, K. M., Yule, D., McPhillips, D., McNeil, J. C., & Pace, A. (2018, 08). Preliminary ages of prehistoric earthquakes on the Banning Strand of the San Andreas Fault, near North Palm Springs, California. Poster Presentation at 2018 SCEC Annual Meeting.

Related Projects & Working Groups
San Andreas Fault System (SAFS)

Ages of Prehistoric Earthquakes on the Banning Strand of the San Andreas Fault, Near North Palm Springs, California

Bryan A. Castillo, Sally F. McGill, Katherine M. Scharer, Doug Yule, Devin McPhillips, James C. McNeil, Sourav Saha, Nathan D. Brown, & Seulgi Moon

Submitted August 7, 2019, SCEC Contribution #9361, 2019 SCEC Annual Meeting Poster #134

The southernmost section of the San Andreas Fault (SAF) is the only section of that fault that has not ruptured in the last 200 years. It is not known whether this long quiescent period reflects a long average recurrence interval for this portion of the fault or whether the current interseismic interval is longer than average. Near Indio, the SAF splits into 3 strands; limited paleoseismic work has been conducted on the Mission Creek and Garnet Hill strands and the Banning strand has no available age control for any surface-rupturing prehistoric earthquakes. We studied a paleoseismic trench that was excavated across the Banning strand by Petra Geosciences (33.9172°, -116.538°). The trench exposed a ~40 m-wide fault zone in interbedded alluvial sand and gravel, coarse-grained debris flow deposits, and clay-silt deposits. We present the first paleoseismic record for the Banning strand of the southern SAF. The most recent event occurred between 730 and 950 cal BP, potentially coincident with rupture of the San Gorgonio Pass Fault Zone. We interpret that five earthquakes have occurred since 3.3-2.5 ka and eight earthquakes have likely occurred since 7.1-5.7 ka. It is possible that additional events may have occurred without being recognized, especially in the deeper section the stratigraphy, which was not fully exposed across the fault zone. We calculate an average recurrence interval of 380 - 640 yrs based on four complete earthquake cycles between earthquakes 1 and 5. The average recurrence interval is thus equivalent to or less than the elapsed time since the most recent event on the Banning strand. The recurrence interval is similar to that of the San Gorgonio Pass Fault Zone (450-1850 years) but longer than that for the Mission Creek strand (~220 years).

Key Words
San Andreas Fault, Banning strand, Paleoseismology

Citation
Castillo, B. A., McGill, S. F., Scharer, K. M., Yule, D., McPhillips, D., McNeil, J. C., Saha, S., Brown, N. D., & Moon, S. (2019, 08). Ages of Prehistoric Earthquakes on the Banning Strand of the San Andreas Fault, Near North Palm Springs, California. Poster Presentation at 2019 SCEC Annual Meeting.

Related Projects & Working Groups
San Andreas Fault System (SAFS)

GC13A-06 - Inferring sediment dynamics using single-grain feldspar post-IR IRSL luminescence dating in southern California, North America

Monday, 9 December 2019

14:55 - 15:10

Moscone West - 2003, L2

ePoster

Copy and pasted text document 1.txt Download

Swirl Topics

Earth Processes - SWIRL

Abstract

Identifying natural cycles of waxing and waning of sedimentation is crucial to quantify robust recurrence interval (RI) of earthquakes of depositional episodes, which is one of the most important factors for seismic hazard modeling in the tectonically active areas such as southern California, USA. In paleoseismic studies, distinct tectonic behaviors across different fault strands are often assumed for the variation in apparent RI, instead of sedimentary history. However, sediment starvation or intense erosion between earthquake events may result in the absence of clear unconformities, making multiple events appear as one event and add intrinsic biases in the interpretation of paleoseismic events including estimates of average RI. As such, a site with only occasional sedimentation may be masking earthquake events, where perhaps the true RI is lower, but the apparent RI may be higher. It is therefore possible that the variation in the apparent RI is affected by depositional history in some paleoseismic sites, rather than the variations in tectonic activities solely. To test this hypothesis, we are exploring individual feldspar single-grain post-infrared infrared stimulated luminescence (pIR IRSL) and multiple elevated temperature post-IR IRSL (METpIRIR) signals from a trench site on the Banning Strand of the southern SAFS (San Andreas fault system) at 18th Avenue, in N Palm Springs, Coachella Valley, CA. The paleoseismic site represents an alluvial fan-axial valley deposit. At least eight event horizons are identified and dated using 17 feldspars pIR IRSL ages. Fifteen of the total 17 pIR IRSL ages show stratigraphic coherence and correspondence with the youngest detrital charcoal ^{14}C ages at 1-sigma. All the samples, except one, seem partially bleached and may contain grains which were bleached during earlier sediment transport events. At least seven single-grain age sub-populations are identified using the finite mixture model, and these show a potential connection with the alluvial fan incisional ages derived from ^{10}Be dating of boulders on fan surfaces upstream. These results indicate that there is a linkage between climate-driven selective sediment evacuation and aggradation in the study area, which needs to be taken into account when interpreting recurrence intervals from similar paleoseismic sites.

Authors

Sourav Saha
Northern Kentucky University
University of California Los Angeles

Seulgi Moon
University of California Los Angeles

Nathan Brown

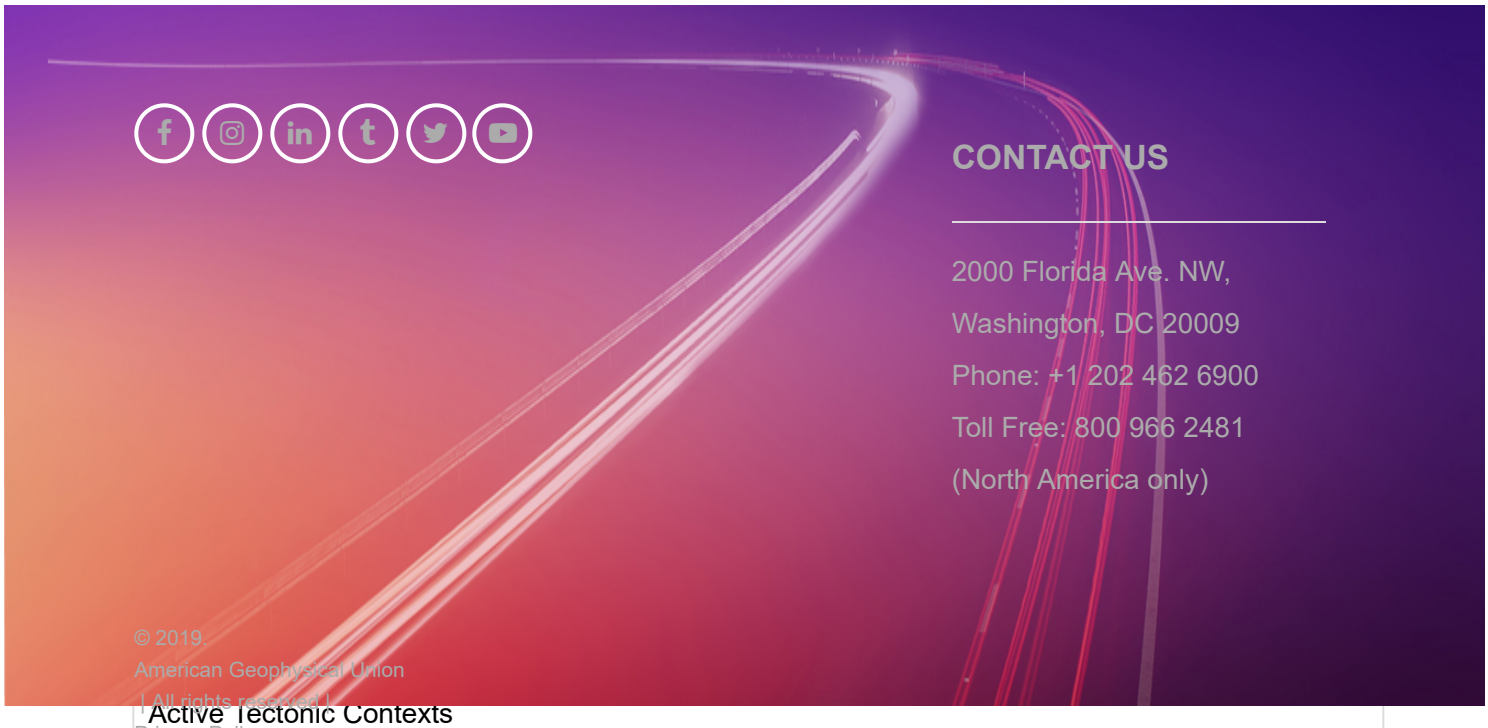

Active Tectonic Contexts

Edward Rhodes, *University of Sheffield, Department of Geography, Sheffield, S10, United Kingdom, Andrew Ivester, University of Sheffield, Department of Geography, Sheffield, United Kingdom, James Francis Dolan, University of Southern California, Department of Earth Sciences, Los Angeles, CA, United States, Russ James Van Dissen, GNS Science, Lower Hutt, New Zealand and Timothy Little, Victoria University of Wellington, School of Geography, Environment and Earth Sciences, Wellington, New Zealand*

Preliminary Results from the Topliff Hill Paleoseismic Site: Evidence for 5-7 Basin and Range Normal Faulting Events in Tooele County, Utah Since the Late Pleistocene

Sally Ward, *Rachel Richards, Brigham Whitney, Nathan A Toke and Michael P Bunds, Utah Valley University, Department of Earth Science, Orem, UT, United States*

Influence of sediment dynamics and alluvial fan formation on paleoseismic studies in southern California, North America

Sourav Saha, Seulgi Moon, Nathan D. Brown, Ed J. Rhodes, Sally F. McGill, Bryan A. Castillo, Katherine M. Scharer, Devin McPhillips, & Doug Yule

Submitted August 13, 2019, SCEC Contribution #9535, 2019 SCEC Annual Meeting Poster #129 (PDF)

Paleoseismic data provide a record of past surface-rupturing earthquakes, but the fidelity of the record depends on the completeness of trench stratigraphy and the precision of geochronology. For example, a period of erosion might scour fault terminations from multiple earthquakes to a single stratigraphic level, leaving evidence of no more than one earthquake in the stratigraphy. On the southern San Andreas Fault System (sSAFS), California, USA, stratigraphic completeness may be of particular concern because many paleoseismic sites are located on alluvial fans, where sediment is deposited episodically and sometimes eroded. Classic cut-and-fill terrace sequences are an end-member example of this behavior, but even a discrete alluvial fan surface has likely experienced hiatuses of years to decades between depositional events. On the sSAFS, previous workers have calculated apparent recurrence intervals (RIs) from trenches on different fault strands and interpreted variable RIs in terms of differences in fault slip rate or other tectonic characteristics. Here, we explore the alternative hypothesis that apparent RIs depend on local depositional history and stratigraphic completeness. To this end, we are in the process of examining individual feldspar single-grain post-infrared infrared stimulated luminescence (pIR IRSL) ages from a trench site on the Banning Strand of the sSAFS at 18th Avenue. The paleoseismic site was in an alluvial fan-axial valley deposit. At least eight earthquake event horizons are identified and dated using 17 feldspar pIR IRSL ages, consisting of approximately 250 grains apiece. Fifteen of these ages show stratigraphic coherence and correspondence with the youngest detrital charcoal 14C ages at 1-sigma. Analysis of over-dispersion indicates that all but one of the samples are partially bleached; this is consistent with limited exposure at the surface and rapid sediment transport prior to deposition at the trench site. At least seven single-grain age sub-populations are identified using the finite mixture model. The ages of these subpopulations appear to correlate with the 10Be-derived ages of terraces in upstream cut-and-fill sequences, potentially recording incision followed rapid deposition a short distance downstream. These results indicate that there is a linkage between climate-driven selective sediment evacuation and aggradation in the study area, which needs to be considered when interpreting RIs from similar paleoseismic sites.

Key Words
Luminescence dating, San Andreas Fault System, Sediment dynamics, Recurrence interval, Paleoseismic, Southern California

Citation
Saha, S., Moon, S., Brown, N. D., Rhodes, E. J., McGill, S. F., Castillo, B. A., Scharer, K. M., McPhillips, D., & Yule, D. (2019, 08). Influence of sediment dynamics and alluvial fan formation on paleoseismic studies in southern California, North America. Poster Presentation at 2019 SCEC Annual Meeting.

Related Projects & Working Groups
San Andreas Fault System (SAFS)